PALACKÝ UNIVERSITY OLOMOUC
FACULTY OF SCIENCE
JOINT LABORATORY OF OPTICS

BACHELOR'S THESIS

Particle resonances in selected data from the ATLAS experiments

Author:	Jan Straka
Study program:	B0533A110007 Applied Physics
Field of study:	1702R001 Applied Physics
Form of study:	Full-time
Supervisor:	Mgr. Jiří Kvita Ph.D.
Date of submission:	August 2023

UNIVERZITA PALACKÉHO V OLOMOUCI
PŘÍRODOVĚDECKÁ FAKULTA
SPOLEČNÁ LABORATOŘ OPTIKY

BAKALÁŘSKÁ PRÁCE

Částicové rezonance ve vybraných datech z experimentu ATLAS

Vypracoval:	Jan Straka
Studijní program:	B0533A110007 Aplikovaná fyzika
Studijní obor:	1702R001 Aplikovaná fyzika
Forma studia:	Prezenční
Vedoucí práce:	Mgr. Jiří Kvita Ph.D.
Termín odevzdání:	Srpen 2023

Declaration

I hereby declare that I have prepared the submitted bachelor's thesis independently under the supervision of Mgr. Jiří Kvita Ph.D. and that I have used the resources cited and listed in the used bibliography.

Signed in on

. . . . . .

Jan Straka

Acknowledgment

I would like to express my sincere gratitude to my supervisor Mgr. Jiří Kvita Ph.D. for the precious time he devoted to our consultations, for his leadership, guidance, all his valuable advice and immense patience he had with me.

Bibliographical identification:

Autor's first name and surname	Jan Straka
Title	Particle resonances in selected data from the ATLAS experiments
Type of thesis	Bachelor
Department	Joint laboratory of optics
Supervisor	Mgr. Jiří Kvita Ph.D.
Consultant	Mgr. Petr Baroň
The year of presentation	2023
Abstract	The bachelor thesis focuses on the analysis of selected data from the ATLAS experiment at the LHC collider. These data are from heavy ion collisions, which are further processed and analyzed by means of custom programs using the ROOT tool in the C++ environment. The analysis constructs four vectors to calculate the invariant masses of the resonances and to identify individual resonance peaks in dilepton decays and subsequently in top quark pair decays.
Keywords	invariant mass, resonances, top quark, Z boson, W boson, charmonium, bottomonium, high energy physics
Number of pages	49
Number of appendices	2
Language	English

Bibliografická identifikace:

Jméno a příjmení autora	Jan Straka
Název práce	Částicové rezonance ve vybraných datech z experimentu ATLAS
Typ práce	Bakalářská
Pracoviště	Společná laboratoř optiky
Vedoucí práce	Mgr. Jiří Kvita Ph.D.
Konzultant	Mgr. Petr Baroň
Rok obhajoby práce	2023
Abstrakt	Bakalářská práce se zabývá analýzou vybraných dat experimentu ATLAS na urychlovači LHC. Jedná se o data ze srážek iontů, která jsou dále zpracovaná a analyzována pomocí vlastních programů za pomocí nástroje ROOT v prostředí C++. Analýza konstruuje čtyřvektory k výpočtu invariantní hmotnosti a identifikaci rezonančních píků v dileptonových rozpadech a následně v rozpadech dvou top kvarků.
Klíčová slova	invariantní hmota, rezonance, top kvark, Z boson, W boson, charmonium, bottomonium, fyzika vysokých energií
Počet stran	49
Počet příloh	2
Jazyk	Anglický

Contents

Introduction

This bachelor thesis focuses on the analysis and invariant mass reconstruction of selected data from the ATLAS experiment at the Large Hadron Collider at CERN (European Organization for Nuclear Research) in Geneva, Switzerland. The thesis is divided into five chapters with the titles: System of Elementary Particles, ATLAS Experiment, Invariant Mass, Main Analysis: Dimuon Decay, Main Analysis: Top Quark Pair Decay.

The first chapter is devoted to a brief introduction to the classification of elementary particles, their fundamental interactions, and the concept of a Standard Model. The ATLAS experiment, its detectors and its coordinate system are described in the second chapter. The third chapter is devoted to the invariant mass and two ways of obtaining it in our analysis.

The fourth and fifth chapters are my analysis of the selected data samples of dimuon decay and top quark pair decay, where I calculate the invariant mass and identify individual resonance peaks using the ROOT software [1].

Chapter 1

System of elementary particles

1.1 Elementary particles classification

An elementary particle, also known as a fundamental particle, is a subatomic particle that exists independently and is not made up of smaller constituents. Elementary particles can be divided into two groups: bosons and fermions, each of group obeying different statistics. Fermions follow the Fermi-Dirac statistics, while bosons follow the Bose-Einstein statistics. Their spin is determined by the spin-statistics theorem: Fermions possess a semi-integer spin and bosons possess an integer spin. Figure 1.1 shows several ways of classifying elementary particles according to their properties, such as spin, generation, charge, mass, or coupling to individual fundamental interactions. [2], [3]

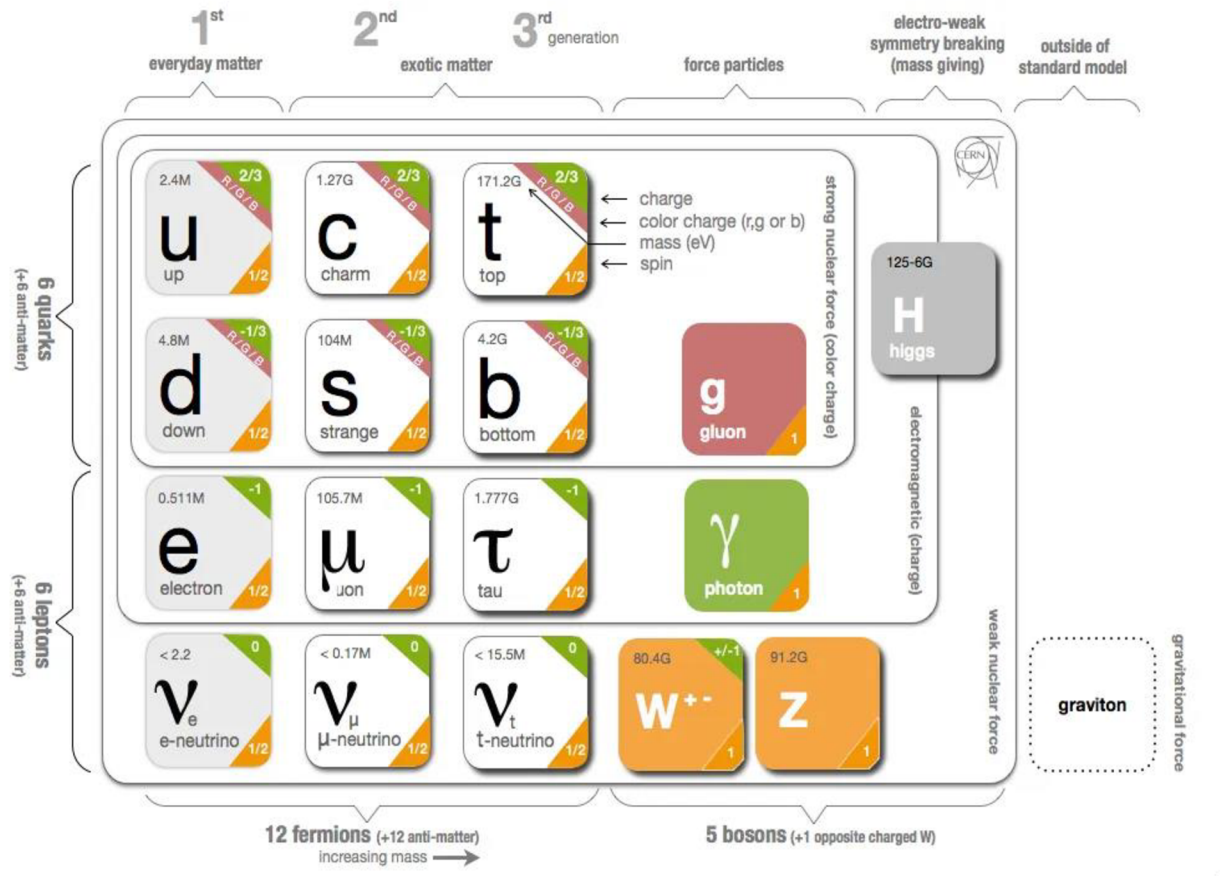

Figure 1.1: Classification of elementary particles by several properties, taken from [4] .

As we can see from Figure 1.1, there are 12 elementary fermions: 6 quarks and 6 leptons (of which 3 are neutrinos), divided into 3 generations of matter particles. There are also elementary bosons (force particles) whose properties assign them to the zones of influence of their interactions: $W^{\pm}$ and Z bosons, which affect flavor-charged fermions; the photon, which affects electrically charged quarks and leptons apart from neutrinos; and the gluons, which affect color-charged quarks. The Higgs boson is not a force particle, but it interacts with every massive particle. There is also an antiparticle to every elementary fermion particle. In addition to elementary particles and their antiparticles, many other particles are composed of quarks. We call them hadrons and divide them into mesons, which are made up of 2 quarks (a quark and its antiquark), and baryons, which are made up of 3 quarks. Hadrons are subject to strong interactions, so the particles they assemble must be colorless. [2], [3]

1.2 Fundamental interactions

Four fundamental interactions (forces) are known to interact with objects in nature according to current knowledge. **The electromagnetic interaction**, to us the most common interaction responsible for all electric and magnetic forces and distribution of electromagnetic radiation. **The gravitational interaction** is another well-known interaction which manifest itself through forces created by mutual interaction of massive objects. Both interactions are forces of long-range, whose effects we can observe and encounter in the macroworld on daily basis. In contrast, **the weak interaction** processes such as β-decays are happening in the microworld**.** **The strong interaction** also dominates in microworld and provides us with the integrity of the atomic nucleus. All four interactions can be thought of mathematically as fields. But only three of them are discrete quantum fields. Their interactions are caused by elementary particles described by the Standard Model of particle physics. However, gravity and the gravitational field are described by Einstein's field equations, which explain the curvature of space-time through Einstein's general theory of relativity. [2], [5], [6]

Table 1: Fundamental interactions and their properties.

Interactions	Coupling constant	Couples to	Range [m]	Exchange particle
Electromagnetic	$\frac{1}{137}$	Electric charge Q	∞ ($\propto r^{-2}$)	photon γ
Gravitational	$6 \cdot 10^{-39}$	Mass m	∞ ($\propto r^{-2}$)	-
Weak	10^{-6}	Weak isospin T_3	10^{-18}	W^+, Z^0, W^-
Strong	1	Color charge C	10^{-15}	gluon, π

Coupling constants have been normalized with respect to the strong interaction.

1.2.1 The electromagnetic interaction

The classical approach explains electromagnetic interaction as a set of electric and magnetic forces interacting with charged objects, summarized in the Lorentz force law. The actions of these forces in electromagnetic fields are described by Maxwell's equations. Quantum electrodynamics, or QED, is the quantum approach to the electromagnetic interaction and a first step to Standard Model of particle physics. The electromagnetic force carried by the photon produces electromagnetic field that causes the attraction between orbital electrons and atomic nucleus, as well as chemical bonding and electromagnetic waves, including visible light. The range of the electromagnetic force is determined by the inverse square law, as it is for the gravitational force. Although the electromagnetic force is much stronger than gravity, as we can see from Table 1.1, the attraction and repulsion of electric charges within large objects tends to cancel each other out, so that gravitational forces dominate over large (astronomical) distances. [2], [7]

1.2.2 The gravitational interaction

The gravitational interaction or gravity is the weakest of the four interactions (Table 1.1). At the atomic scale, where electromagnetic interactions dominate, it is negligible. At the astronomical scale, however, gravity plays the most important, almost exclusive role in describing astronomical objects and their interactions. In analogy with the electromagnetic interaction acting only on electrically charged bodies, gravitation acts only on massive bodies.

The carrier of the gravitational force is postulated to be a hypothetical graviton particle, but only if the gravitational force has a quantum character. Currently, the only theory that can successfully describe the gravitational field is Einstein's general theory of relativity. There is no quantum theory that satisfactorily explains gravity, which separates it from the other interactions present in the Standard Model of particle physics being a quantum model. [2], [7]

1.2.3 Weak interactions

As the uncertainty principle dictates, the weak interaction has the smallest range of all four interactions. Through the exchange of the intermediate vector bosons, the Z boson and the W bosons, the weak interaction can transform one flavor of the quark into another. In the case of radioactive decay, such as β-decays, these flavor transformations cause the proton to become a neutron or the neutron to become a proton. The weak interaction plays the main role in nuclear fission and fusion. Without these processes, the sun would never shine, and heavy nuclei could not be formed. The theory that describes the behavior and effects of the weak force is called quantum flavor dynamics (QFD). However, the term QFD is rarely used because the weak force is better understood by Electroweak Theory (EWT), which is a unification with the electromagnetic interaction. The weak interaction affects both the quarks and the leptons, unlike the upcoming strong interaction, which does not affect the leptons. [2], [3], [7]

1.2.4 The strong interaction

The strongest interaction, which holds the nucleus of an atom together against the enormous repulsive forces of the protons, is the strong interaction. As in the case of the weak interaction, the force carriers are massive particles, so their small range is subject to the limits of the uncertainty principle. The protons and neutrons that build up the nucleus are themselves composed of quarks, and the quarks are held together by the force called the color force. The strong force between the nucleons can be thought of as a residual force of mentioned the color force. In the Standard Model, the basic exchange particle is the gluon caring a color charge and antichange, which mediates the forces among the quarks. The pion, the lightest meson, provides a prediction of the maximum range of the strong force between nucleons. The strong force is described by a theory named Quantum Chromodynamics (QCD), which is part of the Standard Model of particle physics. [2], [8], [7]

1.3 Standard Model

The most important achievement in high-energy physics so far is the Standard Model of particle physics.[6] It is a highly elegant theory that combines the classification of elementary particles according to their respective charges and the fundamental interactions (except gravity) in such a way that describes each particle by a quantum field, while the fundamental forces interact in form of exchange field particles (bosons) among matter particles (fermions). Charge is used here as a specific property of an individual elementary particle, which also defines the fundamental interactions that affect it. For example, photons, bosons of the electromagnetic interaction, couple to electronically charged particles, but gluons, bosons of the strong interaction, couple to color-charged or anticharged particles. Two exceptions apply: The Brout-Englert-Higgs (BEH) field, which behaves in a very special way. As a scalar field, it causes what is known as spontaneous symmetry breaking, which triggers the Higgs mechanism generating mass to all interacting particles. Without the addition of the Higgs mechanism, the boson particles would be considered massless, which has been disproved by measurements. The second exception is the Higgs particle, which can couple with any massive particle (including Higgs particle itself). [6], [5]

Chapter 2

ATLAS Experiment

ATLAS Experiment (A Toroidal LHC ApparatuS) is the largest general purpose particle detector at the LHC (Large Hadron Collider) situated at CERN (the European Organization for Nuclear Research) residing in Switzerland. The LHC has been designed to collide beams of up to 10^{11} protons at a rate of 40 million collisions per second to provide 13.6 TeV (6.8 TeV per beam) proton collisions at a design luminosity 10^{34} $cm^{-2}s^{-1}$. The LHC also provides collisions of heavy ions (pPb, PbPb, XeXe). As a one of the four major particle detectors located at LHC, ATLAS obeys the highest standards of particle detector design because of increased interaction rates, radiation doses, particle multiplicities, energies, and the need for precise measurements. [9], [10]

ATLAS is an enormous and complex cylindrical detector, about 44 meters long, 25 meters high and weighing about 7,000 tons. Positioned around the LHC's collision point, it is designed to detect and analyze the myriad particles resulting from the collision of protons or heavy ions. [9], [10]

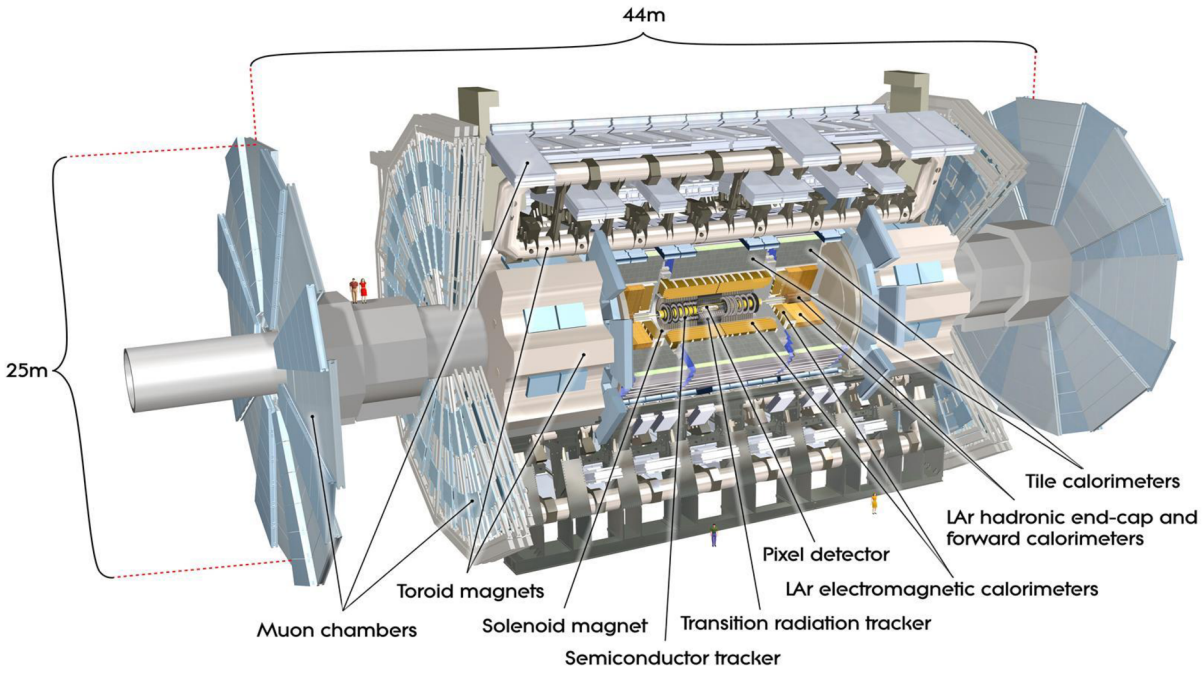

Figure 2.1: The ATLAS detector layout and components, taken from [9] .

As we can see from Figure 2.1, the detector itself consists of several key components, including:

The Inner Detector: The innermost part of ATLAS is the Inner Detector, which is divided into three sub-detectors. **The Pixel Detector**, located just a few centimeters from the bean line, consists of four layers of silicon pixels. Charged particles coming from the collision point deposit a small amount of energy in the pixel detector. This allows the origin and momentum of the particle to be determined to an accuracy of 10 μm. **The Semiconductor Tracker (SCT)** is used to identify and reconstruct the trajectories of charged particles resulting from collisions. It consists of silicon sensors optimized in layers, with particles crossing over at least four of them. **The Transition Radiation Tracker (TRT)** consists of 300,000 thin-walled drift tubes. The tubes contain a mixture of gases that ionize when a particle passes through, producing a detectable electrical signal. This is used to identify the type of particle that has passed through. [9], [10]

The Liquid Argon (LAr) Calorimeter, which surrounds the ATLAS inner detector, is used to measure the energy of electrons, photons, and hadrons. It consists of accordion-like layers of metallic materials (tungsten, copper, or lead) interleaved with a honeycomb structure filled with liquid argon. This construction ensures that incoming particles are detected and converted into a shower of new particles of reduced energy. In this arrangement, the particles induce ionization in the interstitial liquid argon, generating an electric current that can be quantified. The sum of all the currents detected gives the energy of the primary particle that hit the detector. To maintain the liquid state of the argon, the calorimeter operates at a cool -184°C. [9], [10]

The Hadronic Calorimeter (HCAL): The HCAL is designed to measure the energy of the hadrons, such as protons and neutrons, which do not deposit all their energy in the LAr Calorimeter. It consists of alternating layers of plastic scintillating tiles and steel absorber. When the particles hit the steel layers, they are transformed into a shower of new particles. The plastic scintillators then generate photons, which are converted into an electric current. The magnitude of this current is directly proportional to the energy of the original particle. Consisting of approximately 420,000 synchronized plastic scintillator tiles, the Hadronic Calorimeter has the distinction of being the heaviest component of the ATLAS experiment, weighing nearly 2900 tons. [9], [10]

The Muon Spectrometer: The outermost part of ATLAS, the Muon Spectrometer, tracks the momentum of the muons (2nd generation leptons). Five different detector technologies are implemented: **Thin Gap Chambers**, **Resistive Plate Chambers**, **Monitored Drift Tubes**, **Small-Strip Thin Gap Chambers** and **Micromegas**.

Monitored Drift Tube (MDTs) detectors consist of aluminum tubes, each 3 cm wide, containing a gas mixture. When muons pass through these tubes, they release electrons from the gas. These released electrons then drift towards a central wire in the tube, generating a signal. An assembly of more than 380,000 aluminum tubes is meticulously arranged in multiple layers, allowing the trajectory of each muon to be precisely tracked.

The Resistive Plate Chambers (RPCs) consist of pairs of parallel plastic plates held at different electrical potentials with a gas-filled space between them. **The Thin Gap Chambers (TGCs)** consist of parallel 30 μm wires immersed in a gas mixture. In both types of chambers, muons are detected by gas ionization, which triggers the emission of a signal.

For the high-intensity LHC collisions, two other technologies are added: **Micromegas** and **Small-Strip Thin-Gap Chambers (sTGCs).** These advanced detectors are characterized by their ability to track muons quickly and accurately in densely populated areas on either side of the experiment, positioned close to the LHC beamline. [8], [9], [10]

The Magnet System: The ATLAS uses the technique of bending the tracks of charged particles to measure their momentum and charge. This complex process involves the use of two different categories of superconducting magnet systems (solenoidal and toroidal) cooled to a temperature of about 4.5 K. The heart of the ATLAS experiment is the solenoidal magnet, which surrounds the inner detector. This massive magnet is 5.8 meters long, 2.56 meters in diameter, weighs more than 5 tons and generates a magnetic field of 2 Tesla. Using an array of eight coils, the ATLAS toroids generate a magnetic field of 3.5 Tesla, which is used to quantify the muon momentum. There are three toroidal magnets in ATLAS: a pair at the ends of the experiment and another in the core, the largest toroidal magnet ever built. [9], [10]

2.1 Coordinate system in ATLAS detector

To precisely identify and locate the interactions of the particles produced in the LHC collisions, the ATLAS detector uses a coordinate system, which is essential for the accurate reconstruction of particle trajectories and the measurement of their properties.

2.1.1 Cylindrical Coordinates and Cartesian Coordinates:

It is a standard practice in particle physics to use a coordinate system tailored to the geometry of the detector; ATLAS has cylindrical symmetry. The detector uses a right-handed coordinate system with the origin at the nominal collision point. The z-axis is oriented along the beamline and represents the direction of motion of the colliding particles. The azimuthal angle (φ) is measured in the transverse plane perpendicular to the beamline and ranges from 0 to 2π radians. The polar angle (θ) is measured with respect to the z-axis and ranges from 0 to π radians. It provides information about the tilt of a particle's trajectory relative to the beam axis.

In addition to the polar angle and the azimuthal angle, the Cartesian coordinate system (x, y, z) is used to describe particle positions within the ATLAS detector. The x and y axes lie in the so-called transverse plane, perpendicular to the beam axis, while the z axis coincides with the beam axis itself, with the positive x axis defined as pointing from the interaction point to the center of the LHC ring and the positive y axis pointing in an upward direction. Figure 2.2 summarizes the ATLAS coordinate system. [9], [10],[11]

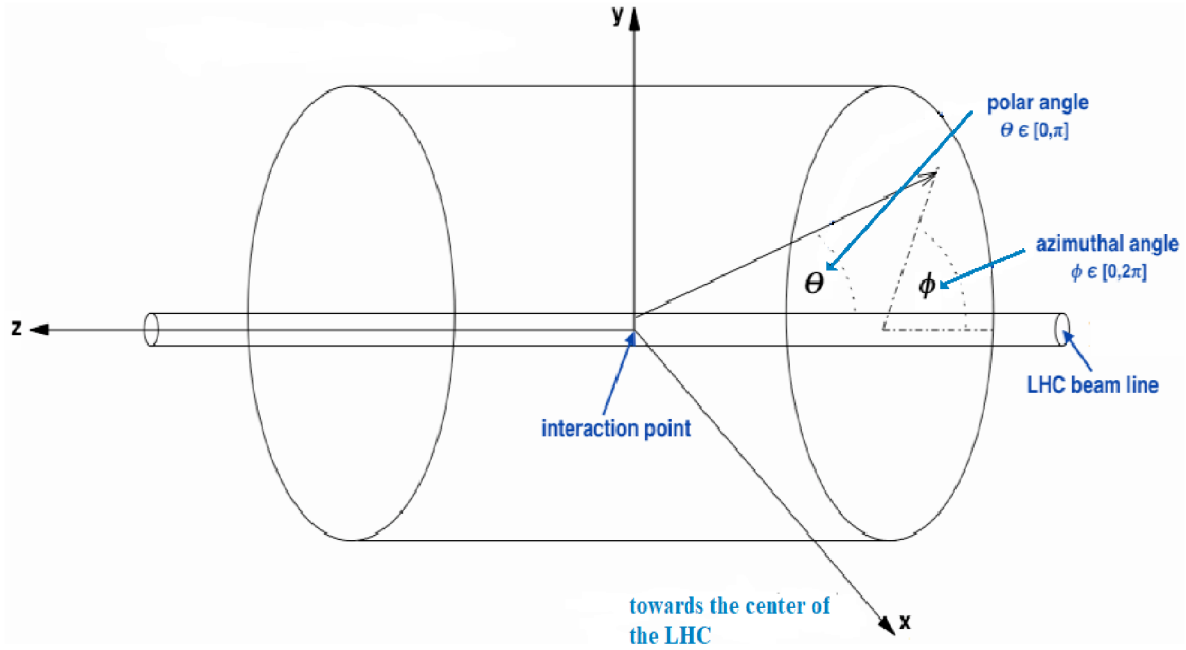

Figure 2.2: Overview of ATLAS coordinate system, adapted from [11].

2.1.1 Rapidity and Pseudorapidity

Regarding high-energy particles with relativistic velocities, it is convenient to define a quantity called rapidity (w). We will assume relativistic expressions for energy and scalar momentum of non-zero mass m:

$$E = \gamma mc^2, \tag{2.1}$$

$$\|\boldsymbol{p}\| = \gamma mv, \tag{2.2}$$

where γ is the Lorentz factor, which equals to $\gamma = \frac{1}{\sqrt{1-\frac{v^2}{c^2}}}$ and c is speed of light constant.

From the relativistic definition the w is given:

$$w = \tanh^{-1}\frac{v}{c} \tag{2.3}$$

and therefore with:

$$\cosh w = \cosh\left(\tanh^{-1}\frac{v}{c}\right) = \frac{1}{\sqrt{1-\frac{v^2}{c^2}}} = \gamma, \tag{2.4}$$

$$\sinh w = \sinh\left(\tanh^{-1}\frac{v}{c}\right) = \frac{\frac{v}{c}}{\sqrt{1-\frac{v^2}{c^2}}} = \frac{v}{c}\gamma, \tag{2.5}$$

the energy and scalar momentum can be represented by the formulas:

$$E = \gamma mc^2 \cosh w, \tag{2.6}$$

$$\|\boldsymbol{p}\| = \gamma mv \sinh w. \tag{2.7}$$

Thus, from the measured energy and momentum, velocity can be expressed as:

$$w = \tanh^{-1}\frac{\|\boldsymbol{p}\|c}{E} = \frac{1}{2}\ln\frac{E+\|\boldsymbol{p}\|c}{E-\|\boldsymbol{p}\|c} = \ln\frac{E+\|\boldsymbol{p}\|c}{mc^2}. \tag{2.8}$$

Nevertheless, in experimental particle physics, the definition of rapidity (y) with respect to a beam axis is commonly used as follows

$$y = \frac{1}{2}\ln\frac{E+p_z c}{E-p_z c}, \tag{2.9}$$

where p_z is the momentum along the beam axis. When a highly relativistic particle scatters in a direction perpendicular to the beamline, component of the momentum vector p_z will be small and the rapidity will be almost zero. However, assume that the same highly relativistic particle is scattered at a small angle, so the energy will be proportionate to p_z, then the velocity will

approach plus or minus infinity, depending on the direction of the particle in the beamline. [8], [10],[11]

Obtaining the momentum p_z, and total energy E to evaluate the rapidity y for highly relativistic particles scattered along the beam pipe proves to be a challenging task. As a solution to this difficulty, the concept of pseudorapidity η arises. Pseudorapidity is a quantity derived by approximation of the total energy E for highly relativistic particles:

$$y \approx \eta = -\ln \tan \frac{\theta}{2}, \quad \text{for } m \ll E. \tag{2.10}$$

The expression is restricted to almost massless particles, it can also be observed that the pseudorapidity is a function of θ only, so for high energy so called ultra-relativistic particles, its common to went with η instead of θ making it more suitable for high-energy collisions. The range of η is -∞ to +∞, particles close to the beam pipe ($\theta \approx 0°$) have $\eta \approx +\infty$, while particles traveling in the opposite direction ($\theta \approx 180°$) have $\eta \approx -\infty$. [8], [9], [10], [11]

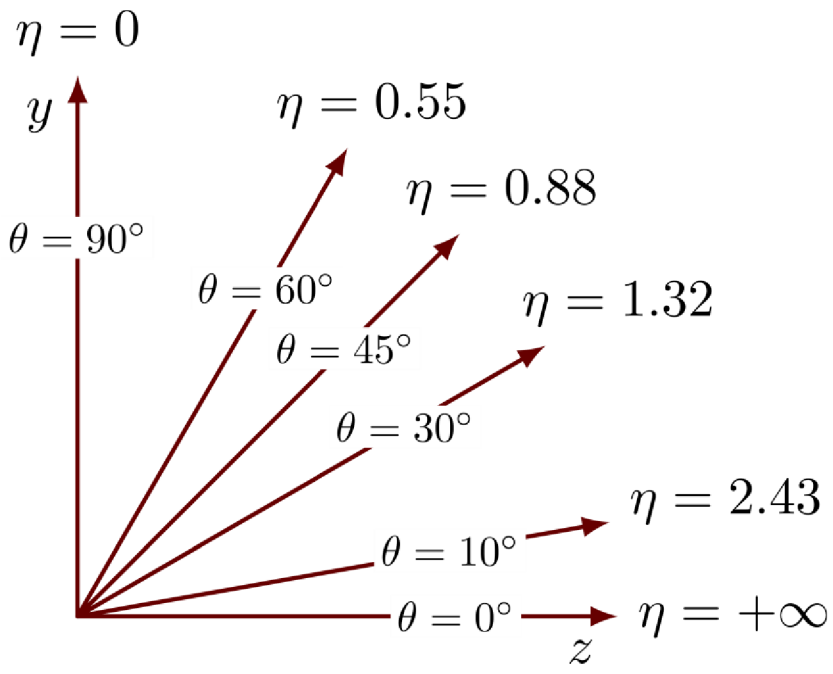

Figure 2.3: Pseudorapidity and theta values on y-z plane, taken from [12].

2.1.2 Transverse Momentum (p_T) and Transverse Energy (E_T):

Transverse momentum (p_T) refers to the momentum component of a particle that is perpendicular to the beam axis. It provides information about the momentum of the particle in the plane transverse to the direction of the colliding beams. Since the beam collision axis defines the z-axis, the transverse momentum is calculated in the x-y plane. Thanks to the transverse momentum, the rapidity with respect to a beam axis is also formulated as:

$$y = \ln \frac{E + p_z c}{\sqrt{m^2 c^4 + p_T^2 c^2}}. \quad (2.11)$$

The transverse energy (E_T) is analogous to the transverse momentum but applies specifically to particles that have no mass or negligible mass compared to their energy. It is calculated in the same way as the transverse momentum, but instead of considering the momentum of the particle, it focuses on the energy component of the particle perpendicular to the beam axis. The transverse energy is particularly relevant for massless or near-massless particles such as photons. [8], [9], [10],

In the ATLAS experiment, in addition to the transverse momentum and energy, there is also an important quantity known as **the missing transverse energy (E_T^{miss}).** The missing transverse energy (E_T^{miss}) represents the imbalance of the transverse momentum in a collision event. In a particle collision, the total momentum in the transverse plane should be conserved. However, some particles, such as neutrinos or potential new invisible particles, may not be directly detected by the ATLAS detector. These undetected or 'missing' particles can carry energy and momentum in the transverse direction, causing an imbalance. The E_T^{miss} is defined as the negative vectorial sum of the transverse momenta of all the particles that have been detected in the event. E_T^{miss} $_s$ is an essential tool for detecting the presence of invisible particles such are neutrinos. [8], [9] [10],[11]

Chapter 3

Invariant Mass

In this thesis, in which I focus primarily on data analysis and the identification of individual resonances, there is one fundamental physical concept that requires special attention, namely the invariant mass.

Invariant mass is a concept used in physics, particularly in the theory of relativity. It's a property used to describe the mass of a system of particles, such as two colliding particles or a collection of particles. Specifically, invariant mass refers to the mass of a system as measured by an observer, regardless of the observer's motion relative to the system. In a nutshell, no matter how fast the system is moving or how it's oriented in space, the invariant mass remains the same. This contrasts with the 'rest mass' of individual particles, which depends on the observer's frame of reference.

To illustrate this, consider the collision of two particles in a high-energy accelerator such as the LHC. As these particles collide, they may decay into other new particles as a result of the interaction. The total energy and momentum of all the particles before and after the collision are conserved.

In particle physics, the invariant mass is equal to the mass in the rest frame of the particles, and it can be calculated by summing the energies and momenta of all the particles involved in the collision. This sum is then used to determine the invariant mass of the whole system. The formula that defines the invariant mass (M) by the energy–momentum relation:

$$(Mc)^2 = \left(\frac{E}{c}\right)^2 - \|\boldsymbol{p}\|^2, \tag{3.1}$$

more practical in natural units, in which case $c = 1$,

$$M^2 = E^2 - \|\boldsymbol{p}\|^2. \tag{3.2}$$

So, the invariant mass of a system of particles can be calculated from the general formula:

$$M^2 = \sum_i E_i^2 - \|\sum_i \boldsymbol{p}_i\|^2, \tag{3.3}$$

where the sums over the particles in the system. In the aforementioned case of two-particle collision the formula of M^2 in natural units is

$$M^2 = (E_1 + E_1)^2 - \|\boldsymbol{p_1} + \boldsymbol{p_2}\|^2. \tag{3.4}$$

3.1 Pseudorapidity formula

Continuing with the example of two particles, we will try to express the new formula for massless particles in terms of the appropriate quantities measured and made available by the ATLAS detector in its coordinate system. So that we can use this formula later in data analysis.

Let's use the expression (3.4) as a starting point and simplify the expression for massless particles using an approximation $m \ll E$.

Since $m \ll E$, we can approximate the energy of each particle as $E \approx p_i$ for $i = 1, 2$, where p_i is a magnitude of the momentum:

$$M^2 = (p_1 + p_2)^2 - \|\boldsymbol{p_1} + \boldsymbol{p_2}\|^2. \tag{3.5}$$

The square of the sum of the momenta can be expressed as the dot product of the vectors:

$$\|\boldsymbol{p_1} + \boldsymbol{p_2}\|^2 = (\boldsymbol{p_1} + \boldsymbol{p_2}) \cdot (\boldsymbol{p_1} + \boldsymbol{p_2}) = {p_1}^2 + 2\boldsymbol{p_1} \cdot \boldsymbol{p_2} + {p_2}^2. \tag{3.6}$$

Substituting back into the expression:

$$M^2 = {p_1}^2 + 2p_1p_2 + {p_2}^2 - ({p_1}^2 + 2\boldsymbol{p_1} \cdot \boldsymbol{p_2} + {p_2}^2). \tag{3.7}$$

Squared terms cancel each other out:

$$M^2 = 2p_1p_2 - 2\boldsymbol{p_1} \cdot \boldsymbol{p_2}\ . \tag{3.8}$$

The dot product of two vectors can be expressed in terms of their magnitudes and the angle α between them:

$$\boldsymbol{p_1} \cdot \boldsymbol{p_2} = \|p_1\|\|p_2\| \cos\alpha = p_1p_2 \cos\alpha, \tag{3.9}$$

leading to

$$M^2 = 2p_1p_2(1 - \cos\alpha). \tag{3.10}$$

Formula (3.10) is the invariant mass of a system composed of two massless particles whose momenta angle α, but as we know from the second chapter, it is common for high energy particles to replace the polar angles with pseudorapidities. Also, instead of the magnitudes p_1

and p_2, it would be more practical to use the transverse momentum of the measured particles, which is directly available from detectors and can always be found in the LHC data.

Let us therefore express the formula that is more suitable for our purposes, using the relationship between the transverse moment (p_T) and the moment (p) of the particles, as well as the definitions of the pseudorapidity (η) and the azimuthal angle (ϕ) and formula (3.8) as a starting point. [1], [3], [8]

Let's rewrite the formula (3.8) using cartesian coordinates

$$M^2 = 2p_1p_2 - 2(p_{x1}p_{x2} + p_{y1}p_{y2} + p_{z1}p_{z2}) \tag{3.11}$$

Based on the conversion to spherical coordinates, we can write the momentum components as

$$p_x = p \sin\theta \cos(\phi), \tag{3.12}$$

$$p_y = p \sin\theta \sin(\phi), \tag{3.13}$$

$$p_z = p \cos\theta. \tag{3.14}$$

The transverse momentum (in the x-y plane) is then equal to

$$p_T = p \sin\theta. \tag{3.15}$$

We can now reformulate the equation 3.11 using p_T:

$$M^2 = \frac{2p_{T1}p_{T2}}{\sin(\theta_1)\sin(\theta_1)} - 2p_{T1}p_{T2}(\cos(\phi_1)\cos(\phi_2) + \sin(\phi_1)\sin(\phi_2) + \cot\theta_1 \cot\theta_2) \tag{3.16}$$

As mentioned above, for $m \ll E$ pseudorapidity is defined by the equation (2.10). Let's take the hyperbolic sine of both sides of the formula:

$$\sinh\eta = \sinh(-\ln\tan\frac{\theta}{2}). \tag{3.17}$$

Using the property $\sinh(-x) = -\sinh(x)$ and the following identity:

$$\sinh x = \frac{e^x - e^{-x}}{2}. \tag{3.18}$$

We get

$$\sinh\eta = -\frac{1}{2}\left(\tan\frac{\theta}{2} - \frac{1}{\tan\frac{\theta}{2}}\right). \tag{3.19}$$

Thus

$$\sinh\eta = -\frac{1}{2}\left(\frac{\sin\frac{\theta}{2}}{\cos\frac{\theta}{2}} - \frac{\cos\frac{\theta}{2}}{\sin\frac{\theta}{2}}\right). \tag{3.20}$$

Leading to

$$\sinh\eta = \frac{\cos^2\frac{\theta}{2} - \sin^2\frac{\theta}{2}}{2\cos\frac{\theta}{2}\sin\frac{\theta}{2}} = \cot\theta. \tag{3.21}$$

We know that

$$\tan\left(\frac{\alpha}{2}\right) = \frac{1-\cos\alpha}{\sin\alpha} = \frac{1}{\sin\alpha} - \cot(\alpha), \tag{3.22}$$

and from the formula (2.10)

$$\tan\left(\frac{\theta}{2}\right) = e^{-\eta} = \cosh\eta - \sinh\eta. \tag{3.23}$$

So, we can also obtain

$$\cosh\eta - \sinh\eta = \frac{1}{\sin\theta} - \cot(\eta), \tag{3.24}$$

$$\cosh\eta = \frac{1}{\sin\theta}. \tag{3.25}$$

Using formulae (3.21), (3.25) in formula (3.16) together with the following identities:

$$\cos(\alpha - \beta) = \cos\alpha\cos\beta + \sin\alpha\sin\beta, \tag{3.26}$$

$$\cosh(\alpha - \beta) = \cosh\alpha\cosh\beta - \sinh\alpha\sinh\beta, \tag{3.27}$$

We get a pseudorapidity formula for squared invariant mass of two particles:

$$M^2 = 2p_{T1}p_{T2}(\cosh(\eta_1 - \eta_2) - \cos(\phi_1 - \phi_2)) \,. \tag{3.28}$$

3.2 Fourvectors construction

Another powerful tool for reconstructing invariant mass are fourvectors representing the particles involved. Fourvectors are mathematical objects that combine three components of space and one component of time, allowing us to describe the space-time properties of particles in a unified way. These four components are typically represented as (ct, x, y, z), where c is the speed of light, t is time, and (x, y, z) are the three spatial coordinates.

However, in particle physics we use a different type of fourvector, the fourmomentum, which is a mathematical object that combines three components of spatial momentum (p_x, p_y, p_z) and one component of energy (E) into a four-dimensional vector. It is typically

represented as (Ec^{-1}, p_x, p_y, p_z), where c is the speed of light. In this representation, Ec^{-1} is the time component and (p_x, p_y, p_z) are the spatial components of the four-momentum. The invariant mass for system with i particles is then given by the general formula (in natural units):

$$M^2 = (\sum_i E_i)^2 - (\sum_i p_{xi})^2 - (\sum_i p_{yi})^2 - (\sum_i p_{zi})^2, \tag{3.29}$$

where the sums over the particles in the system. For example, for reconstruction of two particle system we would use:

$$M^2 = (E_1 + E_2)^2 - (p_{x1} + p_{x2})^2 - (p_{y1} + p_{y2})^2 - (p_{z1} + p_{z2})^2. \tag{3.30}$$

The main advantage of using fourvectors, namely fourmomentums, is that we can treat particles as mathematical objects that we can add and sum up to just one fourvector, which is very convenient and practical for our analysis. [1], [3]

Chapter 4

Main Analysis: Dimuon Decay

This chapter presents my own analysis of a pre-selected sample of data from the ATLAS p-Pb collisions, focusing on dilepton and, more precisely, dimuon decays. The aim is to reconstruct their invariant mass to identify peaks of individual resonances, thanks to which we can specify which decays are likely to have occurred in these collisions, and to compare the obtained masses of the individual resonances with the precisely measured masses according to [8].

4.1 ROOT - Data Analysis Framework

The selected dataset contains a large amount of information on about 20,000 pre-selected collisions (events), for each of which we were able to find out which particles were captured and what their properties were. To analyze such a large amount of data, we will use the ROOT tool developed by CERN.[1]

ROOT provides a powerful data analysis framework. It is mainly used in high-energy physics experiments but is also applicable in other fields. It is a program and library of tools for data analysis, plotting and visualization of graphs and histograms, and contains a wide range of mathematical and statistical functions necessary for data analysis, fitting and modelling. [1]

ROOT is an object-oriented framework based on a C++ environment, making it easy to create and use complex data structures, but it also provides the possibility of Python and R interfaces, allowing users to interact with the framework using these languages. Multi-core processing and parallelization to speed up computations are fully supported. ROOT is a versatile and widely used tool, making it easy to find manuals, documentation and help from other users. [1]

4.2 The process of the analysis

4.2.1 Preparing the data file and accessing it

We start by loading the data into the ROOT program in the form of a ROOT file (.root). As an object-oriented framework, ROOT has some powerful data structures such as the "**TTree**", which can be thought of as a table with rows representing events and columns representing

"branches" (**TBranch**) that can hold different types of data. Each TBranch is a unique container associated with a data type (e.g. an integer, a float...). The final instance is a **TLeaf**, a “leaf” of a TBranch, which represents a single element of data in the Tbranch. This organization allows efficient Input/Output operations and minimizes the memory footprint. [1]

Since we set up a TTree, we will use the MakeClass method on TTree from data file, which will automatically generate us two files in a C++ environment: **nominal.h** in which the class nominal will be created specifically to our TTree (helps with the declaration of individual variables of TLeafs and listing their TBranches) and **nominal.C** which contains main function with loop through we can iterate over single events. Now our data is organized and easily accessible through the event loop in nominal.C with variables declared in nominal.h. [1]

4.2.2 Plotting the muons properties

As discussed in Chapter 3, the path to the invariant mass reconstruction leads us to particle momentum and energy. The first step in the analysis must be to check all the necessary properties of the particles that will construct the invariant mass, in this case a muon-antimuon pair. Referring to formula 3.28 and the section on the fourvectors, we know that the properties to be checked are: the momentum of the captured particle, given by the transverse momentum (p_{T}), the energy of the particle and two angles: the azimuthal angle ϕ and the pseudorapidity η, which is a function of the polar angle θ.

We use two methods to display these properties: Since the creation of our TTree, a TBrowser method has been available to display the TTree data using histograms created in real time. But first we create our own histograms and fill them with data from the TTree using loops and the graphical interpreter TCanvas. Then we compare our histograms with the TBrowser pre-programmed histograms for each property to check our results.

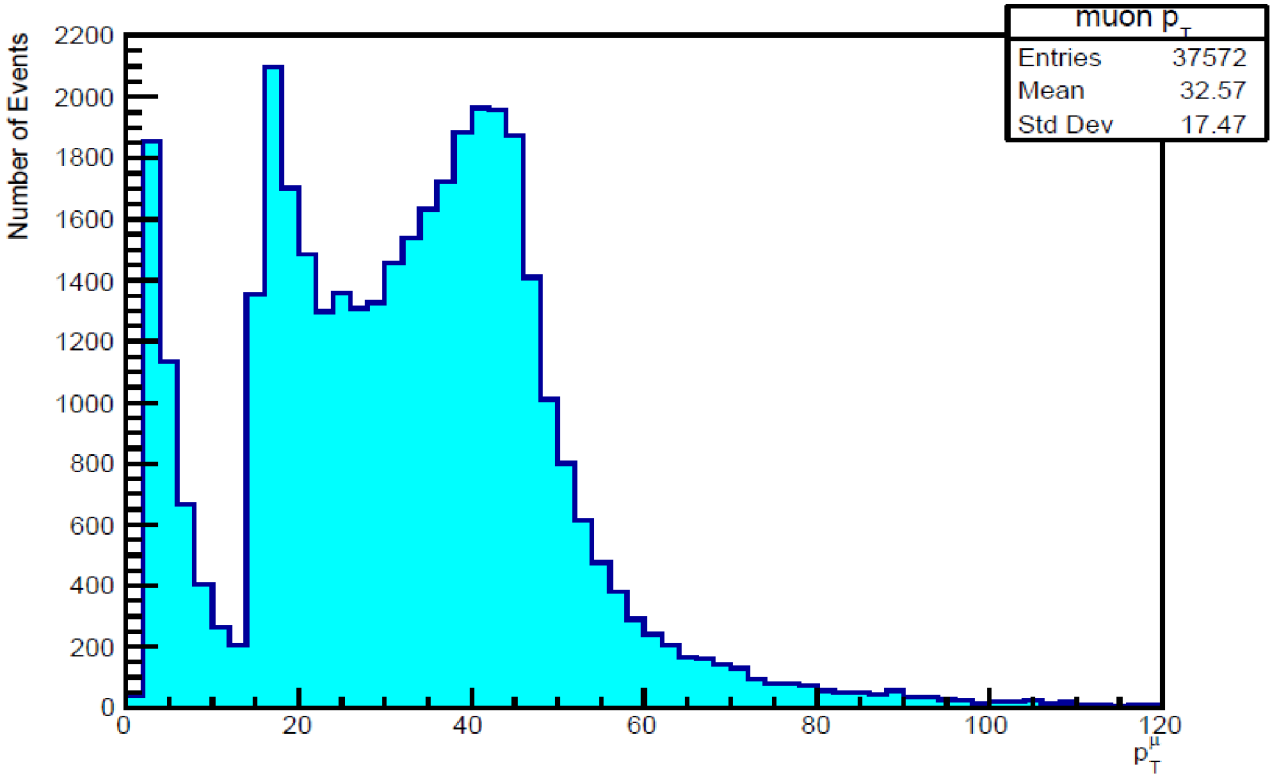

Figure 4.1: Histogram of the p_T of muons in the di-μ sample from ATLAS p-Pb collisions.

4.2.3 Invariant mass reconstruction

After checking the required properties, we proceed to the invariant mass reconstruction. The selected data sample contains information on 18,786 collisions (events) in which, as we can see from Figure 4.1, 37,572 muons were detected, approximately two for each event. We will therefore reconstruct the invariant of the two-particle system. Since the muon is considered to be almost massless in terms of its energy in these events, the pseudorapidity formula 3.28 can be applied. We then obtain the invariant mass by constructing fourvectors.

Using the TMath class, we use formula 3.28 and fill with the values of the given properties of each muon. We then square the resulting invariant masses and use the event loop to fill them into a histogram, which we plot again using TCanvas [1]. As a cross-checking to obtain the invariant mass by fourvectors, we use the class TLorentzvector [1], where we choose two fourvectors definitions: in spherical coordinates (p_T, η, ϕ, E) using η as a function of θ, and in cartesian coordinates (p_x, p_y, p_z, E). Each muon is represented by vector initialized with defined properties. We get the invariant mass by summing them and applying one of the methods of the TLorentzvector class, which returns the invariant mass using a formula similar to 3.30. [1]

In order to use the TLorentzvector defined in Cartesian coordinates, which are not present in the data sample, we need to make a conversion from the given form of the properties using the following equations:

$$p_x = p_{\mathrm{T}} \cos(\phi), \tag{4.1}$$

$$p_y = p_{\mathrm{T}} \sin(\phi), \tag{4.2}$$

$$p_z = p_{\mathrm{T}} \sinh(\eta). \tag{4.3}$$

The reconstruction of the invariant mass was performed once using formula 3.28 and twice using the TLorentzvector class, each time with differently initialized fourvectors, the resulting histograms appeared identical, for verification we construct a 2D histogram for comparison.

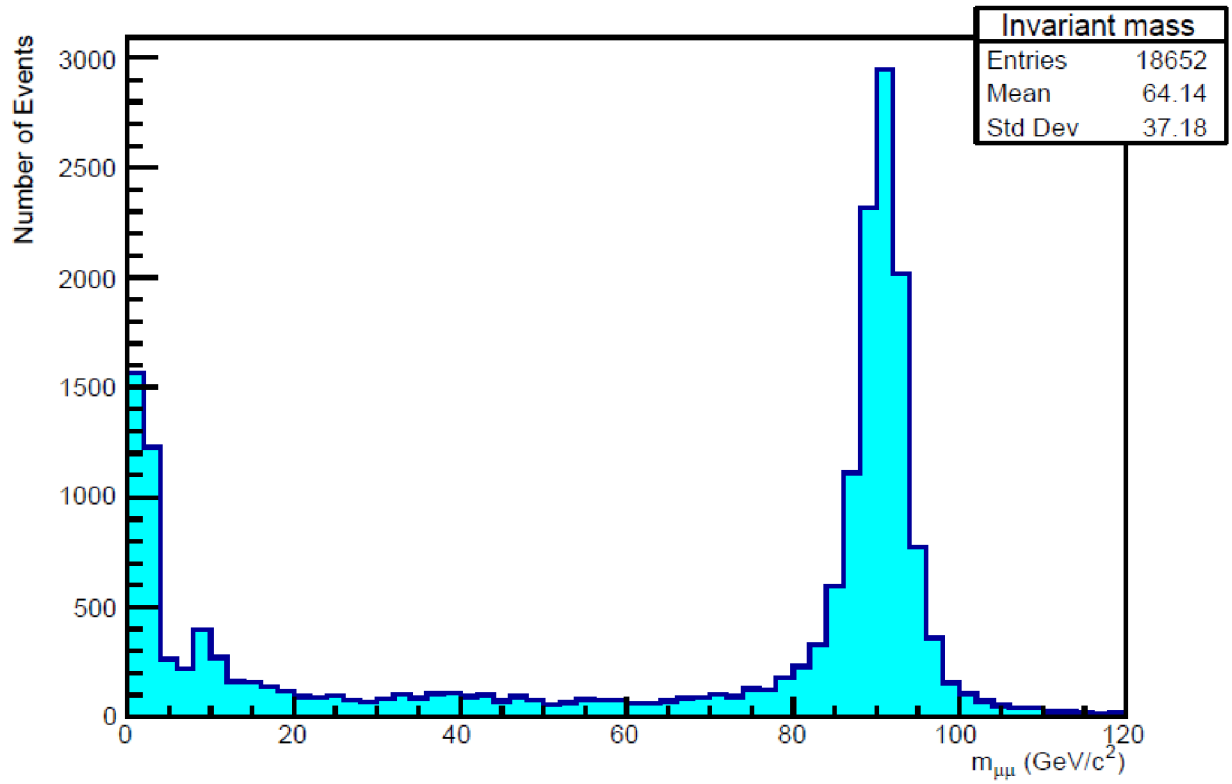

Figure 4.2: Histogram of the invariant mass of muon pairs in the di-μ sample from ATLAS p-Pb collisions.

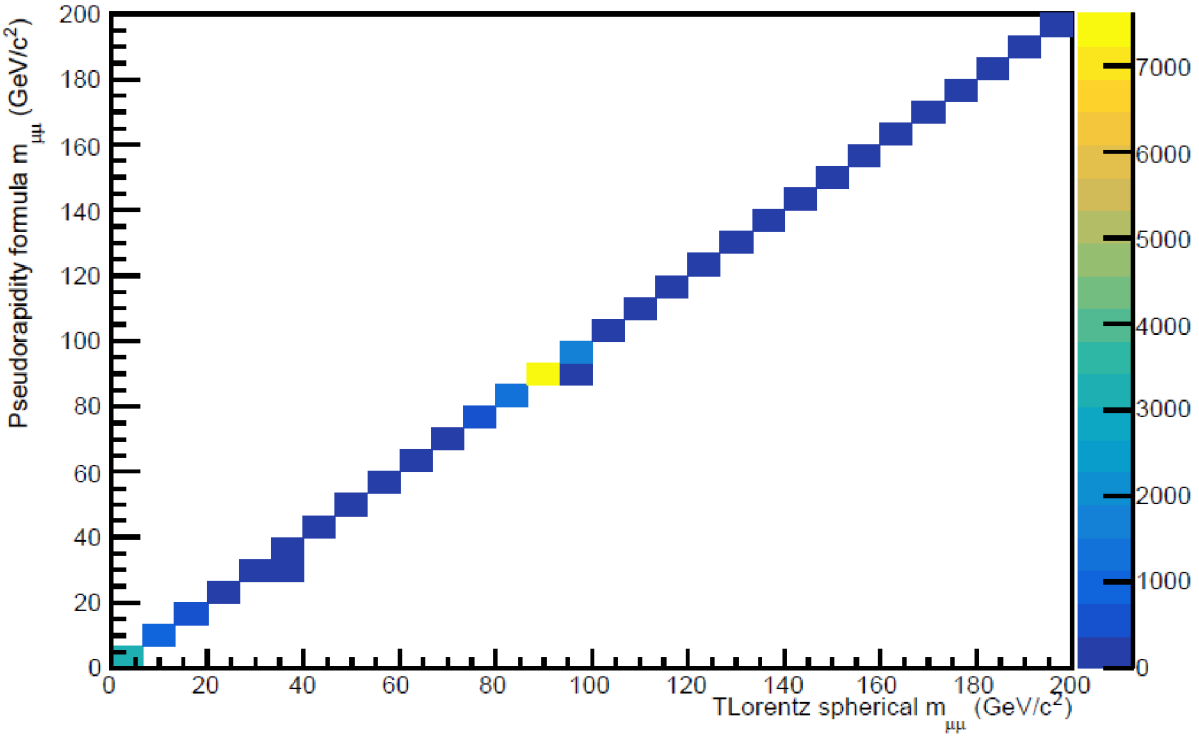

Figure 4.3: 2D histogram of the invariant masses of muon pairs using the pseudorapidity formula and TLorentzvetor (p_T, η, ϕ, E) in the di-μ sample from ATLAS p-Pb collisions.

The use of two differently defined T-Lorentz vectors gave the same results (see Figure 4 in the Appendix). There are very slight differences between the pseudorapidity formula histogram and the TLorentz vector histograms, caused by the approximation in the construction of Formula 3.28. Although the differences are visible in Figure 4.3, they are negligible in terms of identifying the resonances. Therefore, the histogram in Figure 4.2 is validated as the final histogram to be used for further analysis and peak identification. Looking at the histogram, we can see that there is a significant peak between 80-100 GeV/c^2. An interesting structure can also be observed at the beginning of the spectrum between 0-20 GeV/c^2.

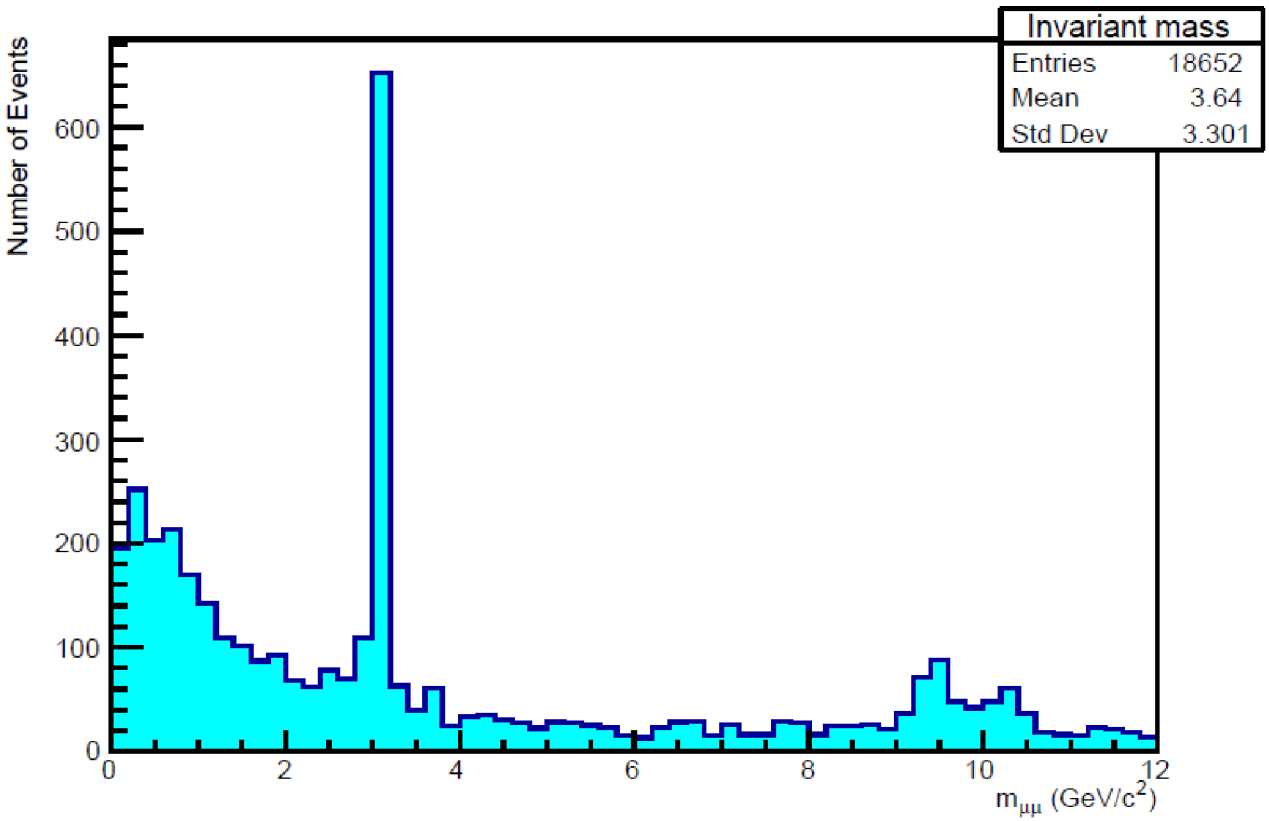

Figure 4.4: Histogram of the invariant mass of muon pairs in the di-μ sample from ATLAS p-Pb collisions, focusing on area between 0-12 GeV/c^2.

Zooming in on this area (Figure 4.4) we can distinguish 4 other peaks, one very distinctive between 2-4 GeV/c^2 and three much less prominent between 8-12 GeV/c^2.

4.3 Identification of resonance peaks

Now that we have successfully found 5 different resonance peaks, it is time to identify them. We localize the individual peaks and fit them with a Gaussian function + constant parameter for background. Gaussian mean parameter gives us the value of the resonance invariant mass and its uncertainty. Knowing the values of the invariant masses, we can then easily identify them and discuss their possible origins.

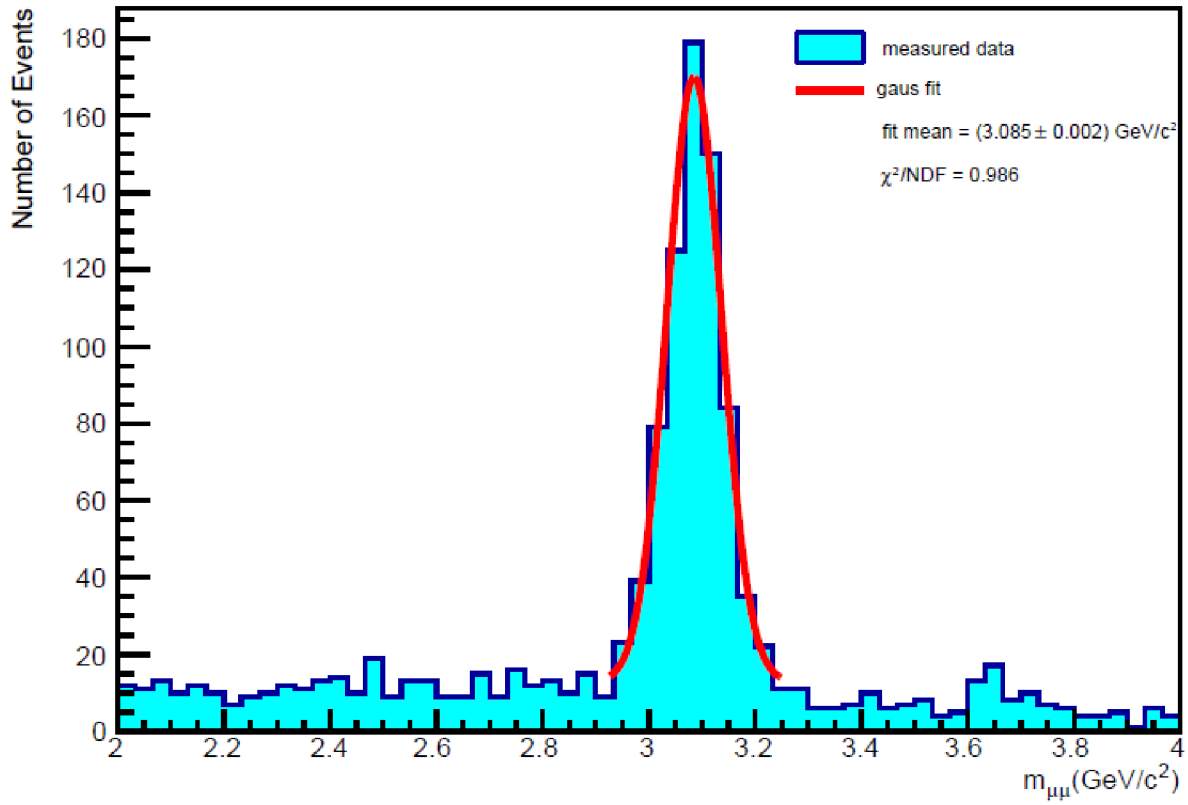

Figure 4.5: Histogram of the invariant mass of muon pairs in the di-μ sample from ATLAS p-Pb collisions, focusing on J/ψ resonance peak localization and fitting. Also indicated is the fit quality in terms of the χ^2/NDF.

Starting with the distinctive peak on figure 4.4 and with the lowest value of the invariant mass, we identify the J/ψ particle (Figure 4.5), which is a meson of a charm and an anticharm quark also known as "Charmonium" and according to the measurements of [8], it has $M_{\mathrm{PDG}} = (3.096900 \pm 0.000006)\ \mathrm{GeV/c}^2$. The mean value of our invariant mass determined by fitting is $M_{J/\psi} = (3.085 \pm 0.002)\ \mathrm{GeV/c}^2$. The quality of fit is given by the $\chi^2/\mathrm{NDF} = 0.986$. The relative deviation of our value with reference to M_{PDG} is about 0.4 %. It can be assumed that

when a J/ψ particle is detected, the decay mode shown in the following Feynman diagram has occurred; according to the source [8], the probability of such a decay is (5.961 ± 0.033) %.

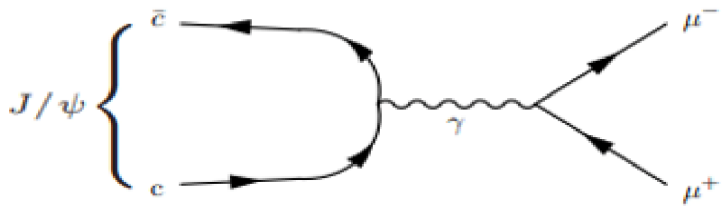

Figure 4.6: Feynman diagram of the J/ψ decay into muon pair, taken from [13].

Following steps are performed to identify three peaks in area between 8-12 GeV/c^2. As can be observed in Figure 4.7, there are three states of a particle called Upsilon ϒ or Bottomonium, since it is a meson composed of a pair of bottom and anti-bottom quarks.

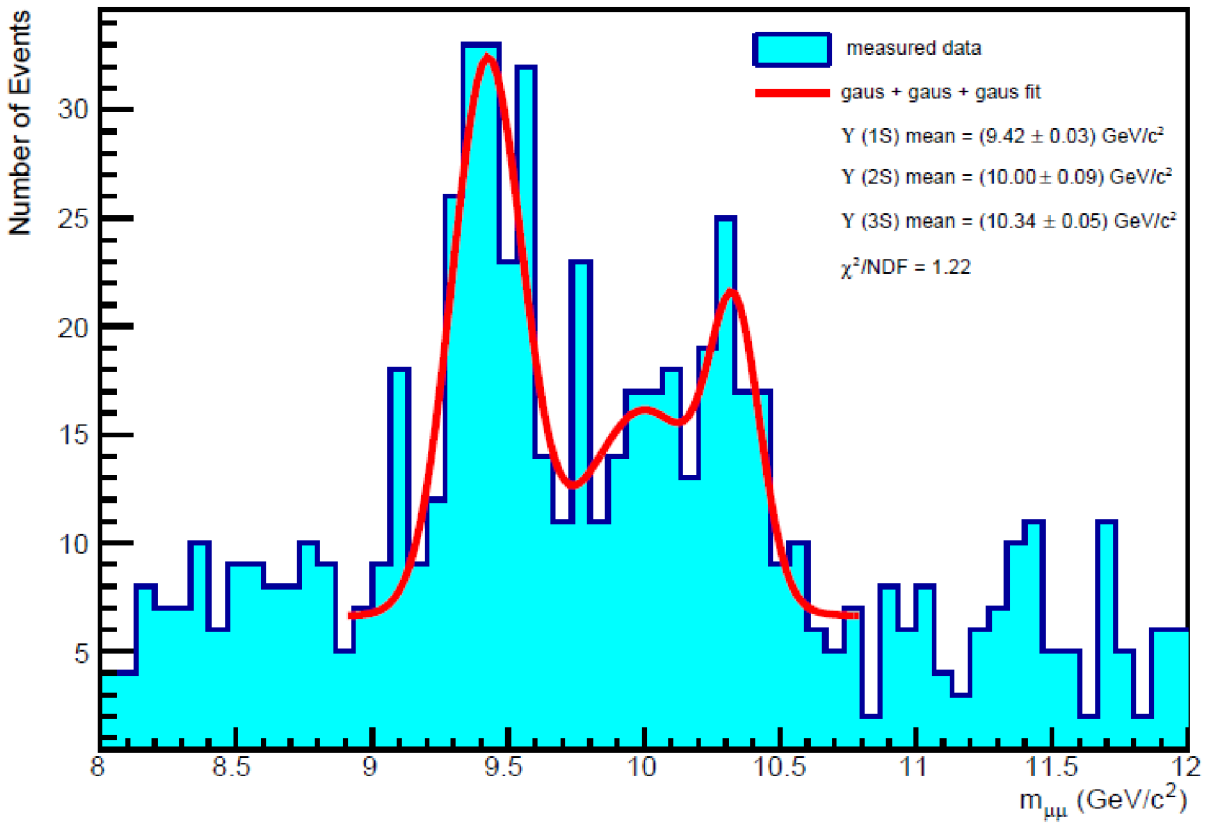

Figure 4.7: Histogram of the invariant mass of muon pairs in the di-μ sample from ATLAS p-Pb collisions, focusing on Bottomonium resonances localization and fitting. Also indicated is the fit quality in terms of the χ^2/NDF.

Specifically, these are the ϒ(1S), ϒ(2S) and ϒ(3S) states, which, according to the measurement of [8] have invariant masses $M_{\mathrm{PDG}}^{1\mathrm{S}} = (9.4604 \pm 0.0001)\ \mathrm{GeV/c}^2$, $M_{\mathrm{PDG}}^{2\mathrm{S}} = (10{,}0234 \pm 0{,}0005)\ \mathrm{GeV/c}^2$ and $M_{\mathrm{PDG}}^{3\mathrm{S}} = (10{,}3551 \pm 0{,}0005)\ \mathrm{GeV/c}^2$. Our mean values of invariant masses are $M_{\Upsilon(1\mathrm{S})} = (9.42 \pm 0.03)\ \mathrm{GeV/c}^2$, $M_{\Upsilon(2\mathrm{S})} = (10.00 \pm 0.09)\ \mathrm{GeV/c}^2$ and $M_{\Upsilon(3\mathrm{S})} = (10.34 \pm 0.05)\ \mathrm{GeV/c}^2$. The quality of fit is given by the $\chi^2/\mathrm{NDF} = 1.22$. The relative deviation of our ϒ(1S) value with reference to M_{PDG} is about 0.4%. The relative deviation of our ϒ(2S) value with reference to M_{PDG} is about 0.2%. Our value for the ϒ(3S) state matches the comparison value within the error interval. By detecting the ϒ mesons we expect the decay mode illustrated in the following Feynman diagram. According to the source [8] the probabilities of such a decays are (2.48 ± 0.04) % for ϒ(1S), (1.93 ± 0.17)% for ϒ(2S) and (2.18 ± 0.21)% for ϒ(3S).

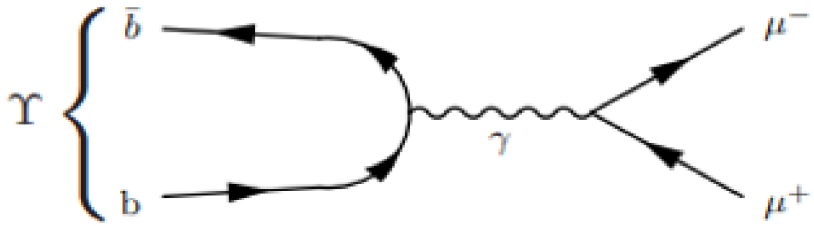

Figure 4.8: Feynman diagram of the ϒ decay into muon pair, taken from [13].

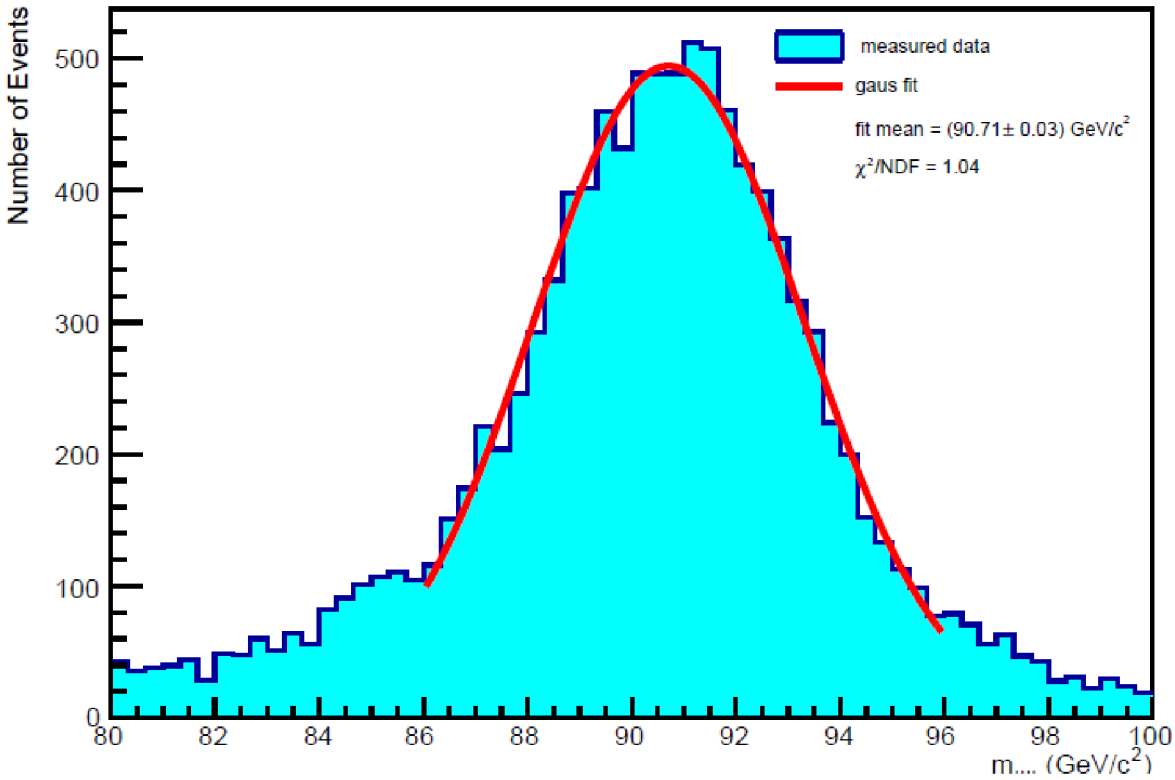

Figure 4.9: Histogram of the invariant mass of muon pairs in the di-μ sample from ATLAS p-Pb collisions, focusing on Z^0 boson localization and fitting. Also indicated is the fit quality in terms of the χ^2/NDF.

The last, most significant, and heaviest peak, visible immediately in Figure 4.2 is the Z^0 boson, which is one of the force carries of weak interaction. According to the measurements of [8] invariant mass of Z boson is $M_{\mathrm{PDG}} = (91.1876 \pm 0.0021)\ \mathrm{GeV/c}^2$, our value determined by fitting is $M_{\mathrm{Z}} = (90.71 \pm 0.03)\ \mathrm{GeV/c}^2$, which gives us the relative deviation about 0.5% with reference to M_{PDG}. The quality of fit is given by the $\chi^2/\mathrm{NDF} = 1.04$. The Z boson can decay directly into a muon pair with the probability (3.3632 ± 0.0042) % according to the [8]. A possible production mechanism can be observed in the following Feynman diagram in Figure 4.10.

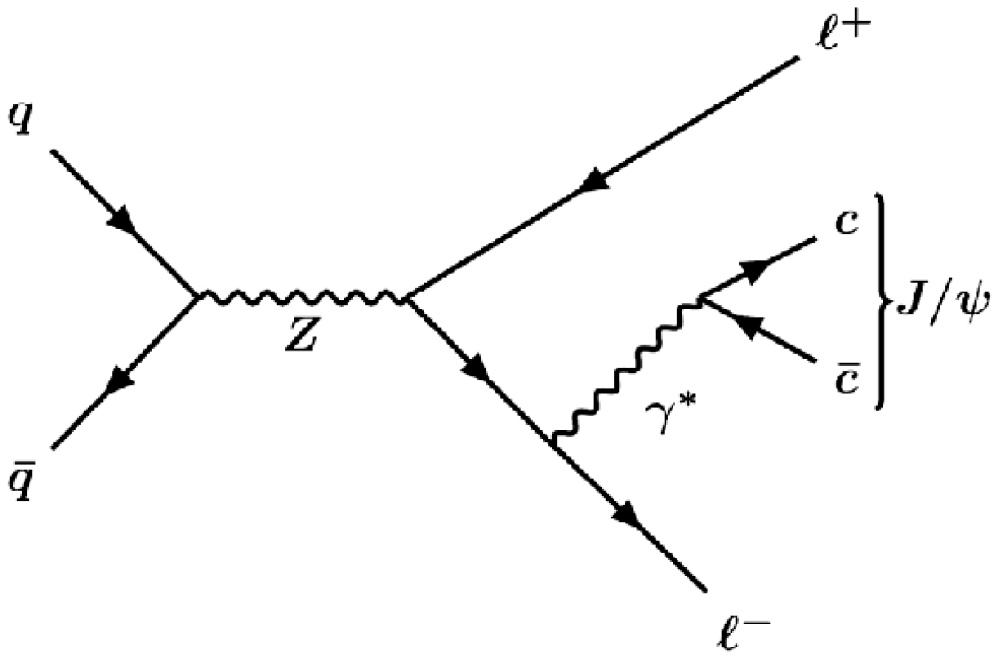

Figure 4.10: Feynman diagram of possible Z^0 production and decay into a lepton pair with additional J/ψ production, taken from [14].

Chapter 5

Main Analysis: Top Quark Pair Decay

This chapter presents my own analysis of a preselected sample of data from the ATLAS detectors, focusing on the production of $t\bar{t}$ pairs and their decays. The aim is to reconstruct the invariant mass of the W boson, which is intermediate to the more complex top quark, whose invariant mass reconstruction will be the main task. We will locate and fit the peaks of the individual resonances and compare the obtained masses with the precisely measured masses according to [4].

5.1 Production of $t\bar{t}$ pairs and their decay modes

In contrast to Chapter 4, we will first look at the production of $t\bar{t}$ pairs and their possible decay modes that we expect to see in the data, which will help us in the correct approach to the analysis itself.

5.1.1 Process of $t\bar{t}$ pairs production

The initial phase of top-pair production in the LHC is the acceleration of two high-energy protons (or heavy ions) along opposing trajectories at velocities approaching the speed of light. At such high energies, the constituents of protons, called partons, carry a significant fraction of the proton's momentum. The exact momentum distribution of partons within protons is described by parton distribution functions. The dominant mechanism to produce top quark pairs at the LHC is the gluon-gluon fusion. In gluon-gluon fusion, the two gluons interact and form a top quark-antitop quark pair ($t\bar{t}$) in the collision. This process exploits the strong force interaction between the gluons. There are also other mechanisms for creating $t\bar{t}$ pairs, such is $q\bar{q}$ annihilation, which are shown in the following Feynman diagrams in Figure 5.1. [8], [15]

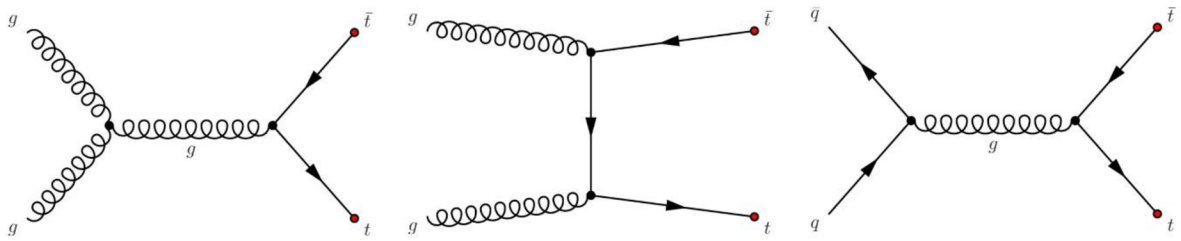

Figure 5.1: Feynman diagrams of top quark pair production: s-channel gluon–gluon fusion, t-channel and s-channel quark–antiquark annihilation, taken from [15].

5.1.2 Expected modes of $t\bar{t}$ pairs decay

Top quark pairs are highly energetic, and they are produced with a combined mass above twice that of a single top quark. They are extremely short-lived and decay quickly via the weak interaction before they can be directly observed. According to [8], in about 99.9% of cases, each top quark decays into a $W^{\pm}$ boson and a bottom quark ($t \rightarrow W^{\pm} + b$). The $W^{\pm}$ bosons from the top quark decay further into different particles, such as leptons and their neutrinos, or hadrons (quark-antiquark pairs), which we observe in the form of jets in our data sample.

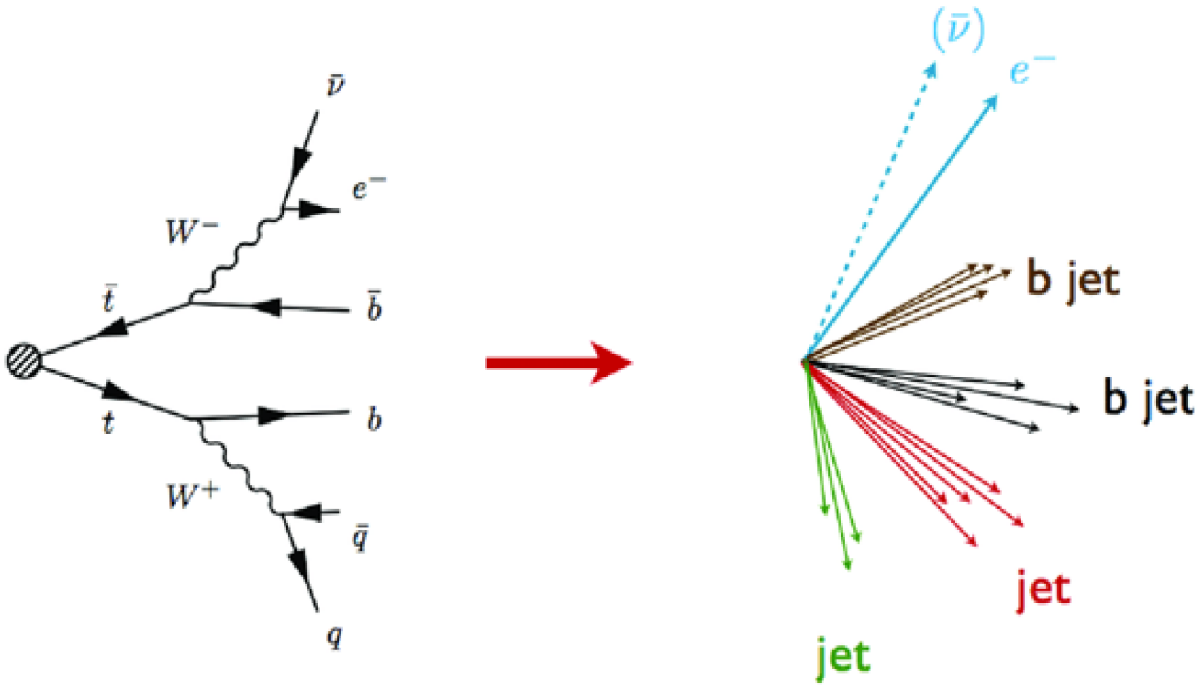

Figure 5.2: Feynman diagram of possible top pair decays with given jet illustration, taken [16].

In our analysis we focus on the decay of the t quark ($t \rightarrow W^{\pm} + b$), whose W boson further decays into jets.

Jets are showers of particles that result from the fragmentation and hadronization of quarks and gluons produced in the collision. As mentioned above, in high-energy collisions, partons can scatter and produce new particles, including quarks and gluons. During the scattering process, the initial quarks and gluons can emit additional gluons and quarks in a process called parton radiation. This radiation is due to the strong force interactions between the partons.

It is well known that quarks and gluons are never observed as isolated particles due to a phenomenon known as confinement. The strong force between quarks and gluons prevents them from existing freely as individual particles. Instead, they rapidly form bound states called hadrons (e.g., protons, neutrons, pions) through a process called hadronization. The quarks and gluons emitted from the initial collision undergo hadronization, forming collimated jets of particles. Together, these jets of hadrons form what is known as a jet. Each jet represents the combined energy and momentum of the original partons and their emitted progeny. Jets typically have a characteristic structure, with a central core (core jet) of high-energy particles surrounded by lower-energy particles in a more diffuse region (jet sheath). The core of the jet is dominated by the highest energy particles produced by the fragmentation of the original quark or gluon. [16]

At the detector level, these jets can be divided into two main categories based on their content: b-tagged jets and light jets.

B-tagged jets are jets containing a B hadron, which is a hadron containing a bottom quark. When a bottom quark is produced in a high-energy collision, it forms a B hadron before eventually decaying into other particles. These B hadrons have relatively long lifetimes and can travel a measurable distance before decaying. Detecting the presence of a B hadron in a beam is known as **'b-tagging'**. [17]

Light jets, on the other hand, are jets that do not contain B hadrons or other heavy hadrons (those containing top or charm quarks). Instead, light jets are produced mainly by the fragmentation of light quarks (up, down and strange quarks) and gluons. These jets are less massive than those containing B hadrons, and their lifetimes are typically too short to be detected directly. As many of the dominant background processes in collider experiments involve light quarks and gluons, they are often used as a background in the search for new physical processes. [16]

5.2 The process of the analysis

This time the data sample analyzed contains 8,581 preselected collisions in which top quark pairs could be produced. Again, the analysis is performed in the ROOT and C++ environments, the advantages of which are described in Chapter 4.

The same procedure for loading data, creating a new **TTree** and generating **nominal.C** and **nominal.h** files as described in Chapter 4 is applied.

5.2.1 Plotting the light jets and the b-tagged jets properties.

This is where the analysis process differs from the previous chapter. As we can see in Figure 5.2, it is necessary to distinguish between light-flavored jets and b-flavored jets. There is a property of each jet captured in the data sample that can tell us whether the jet is considered to be a b-flavored jet, so-called B-tagged, or not. Using conditions with this property and loops, we can iterate over all jets in all events and produce histograms of the properties needed for invariant mass reconstruction, separately for light jets and for b-tagged jets (hereafter referred to as b jets).

There are also majority cases of events where more or less than four jets are detected, including two b jets. We therefore produce histograms of the number of jets and histograms of the number of b jets to help us navigate in the data (see Figures 7,8 in the Appendix). Out of nearly 8,600 events, only about 1050 contain at least 4 jets (including 2 b jets). The most common events are those with 4 light jets and no b jets, such events result from processes such as the production of W+ jets. It should be noted that although there are b jet tagging mechanisms, they only give us a certain probability of whether the jet is really a b jet or not.

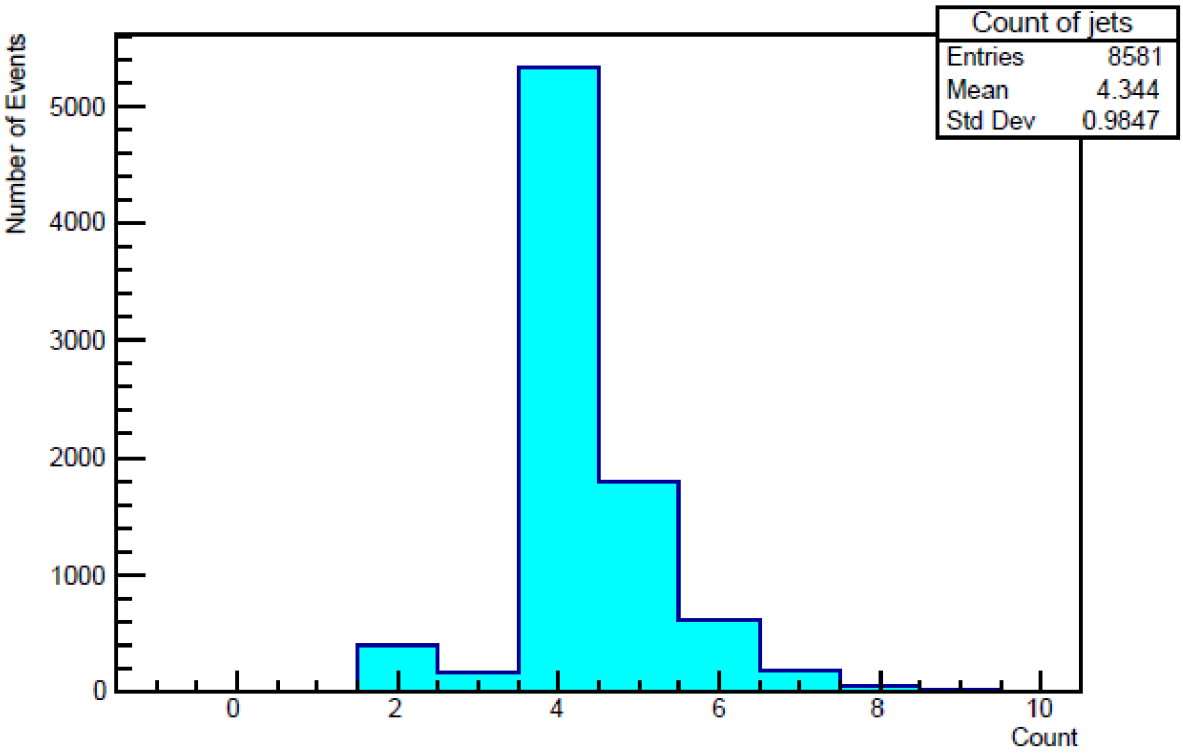

Figure 5.3: Histogram of the counts of light jets in events of the top-quark enriched sample from ATLAS p-Pb collisions.

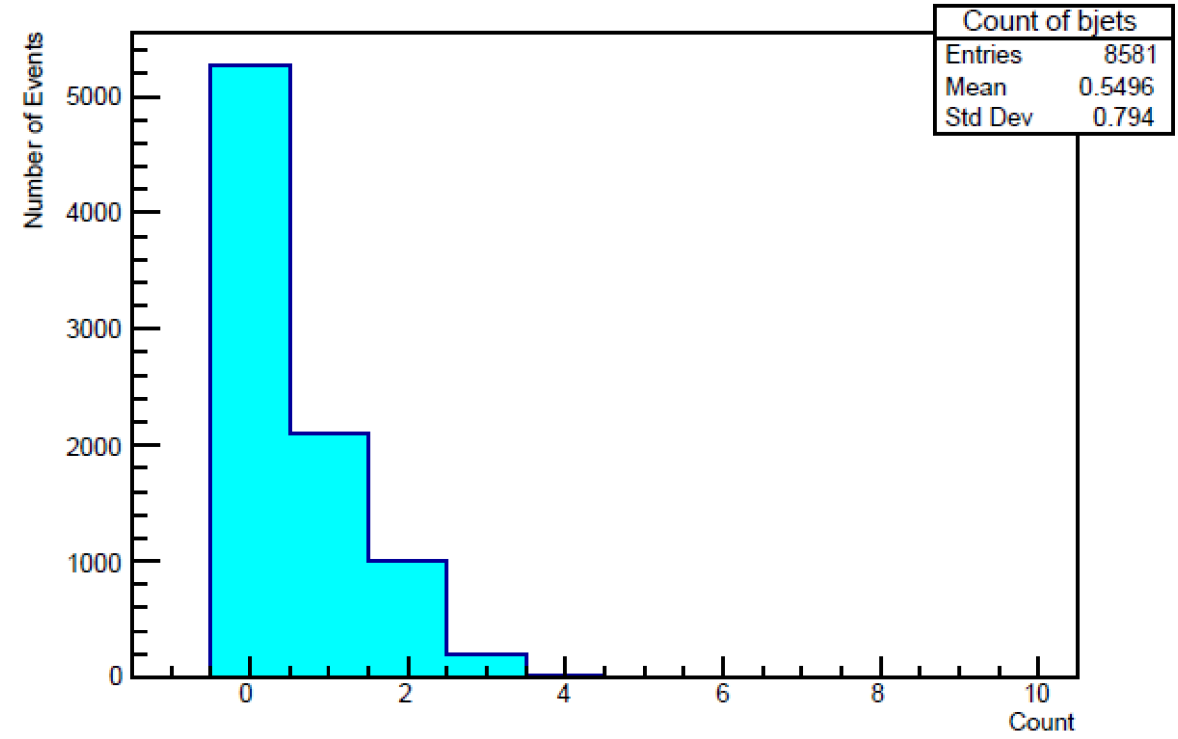

.

Figure 5.4: Histogram of the counts of b jets in events of the top-quark enriched sample from ATLAS p-Pb collisions.

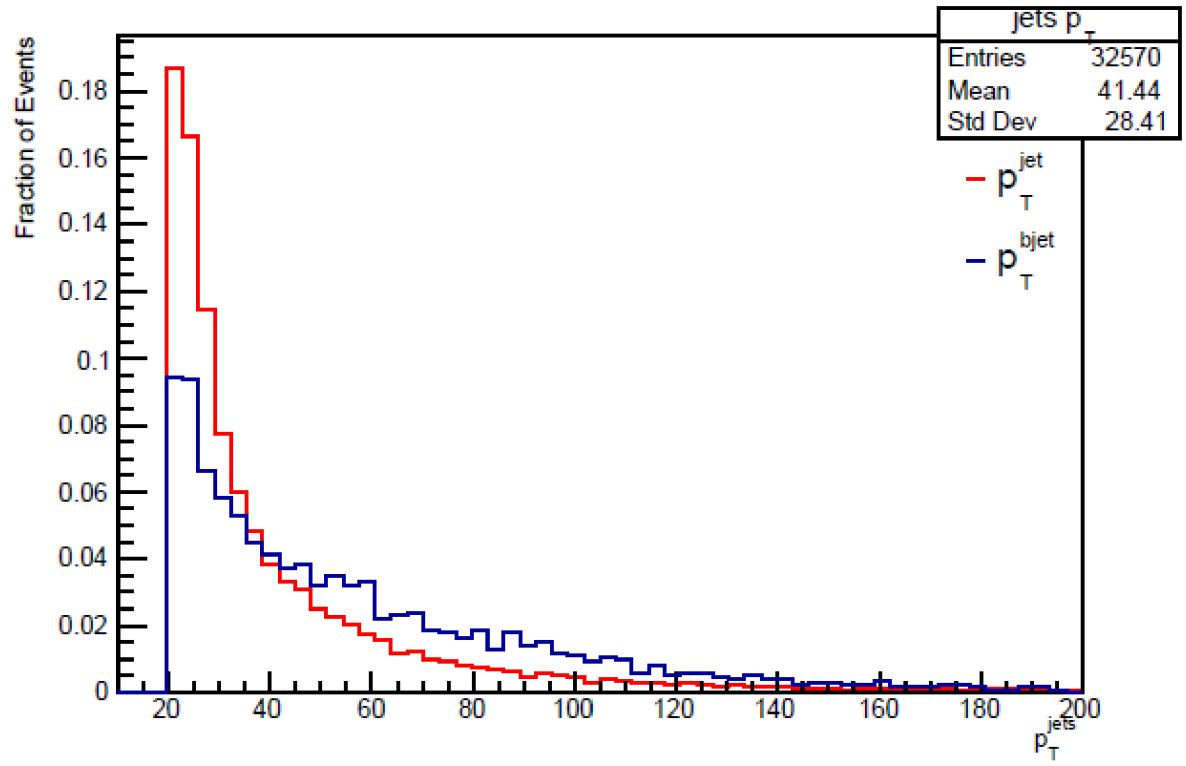

Figure 5.5: Normalized histogram of the p_{T} of light jets and b jets in the top-quark enriched sample from ATLAS p-Pb collisions.

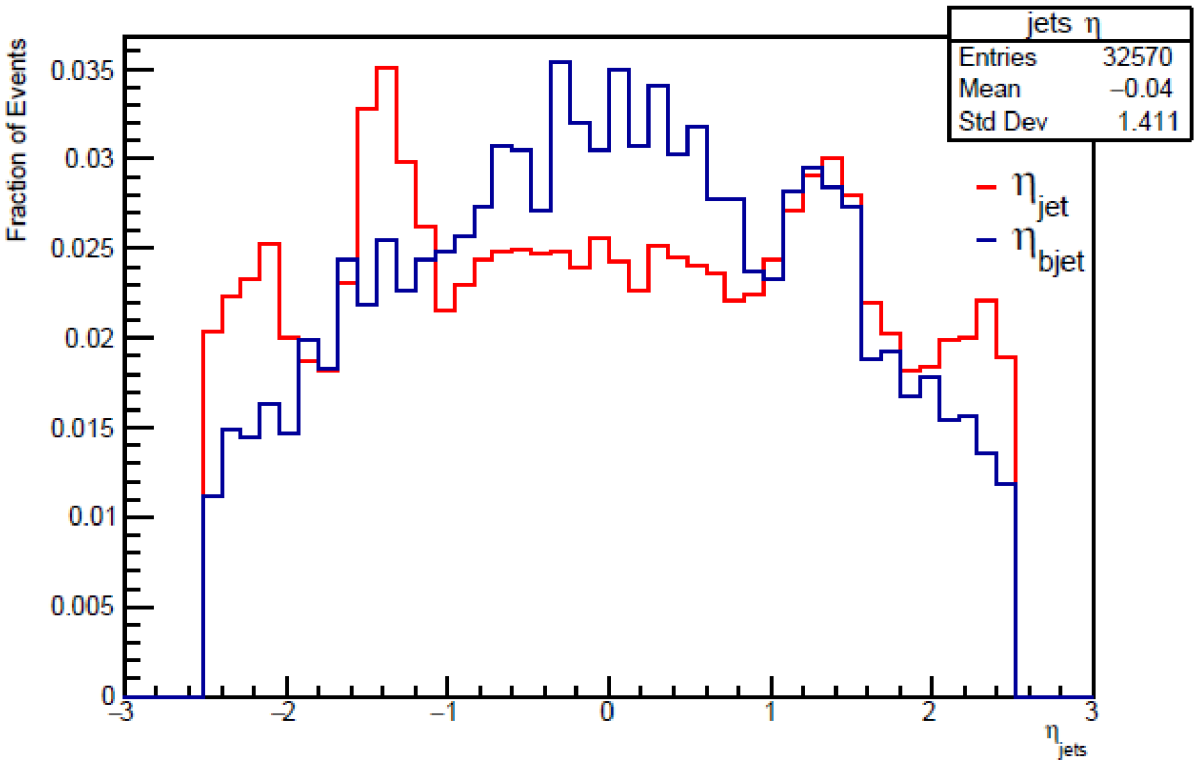

Figure 5.6: Normalized histogram of the η of light jets and b jets in the top-quark enriched sample from ATLAS p-Pb collisions.

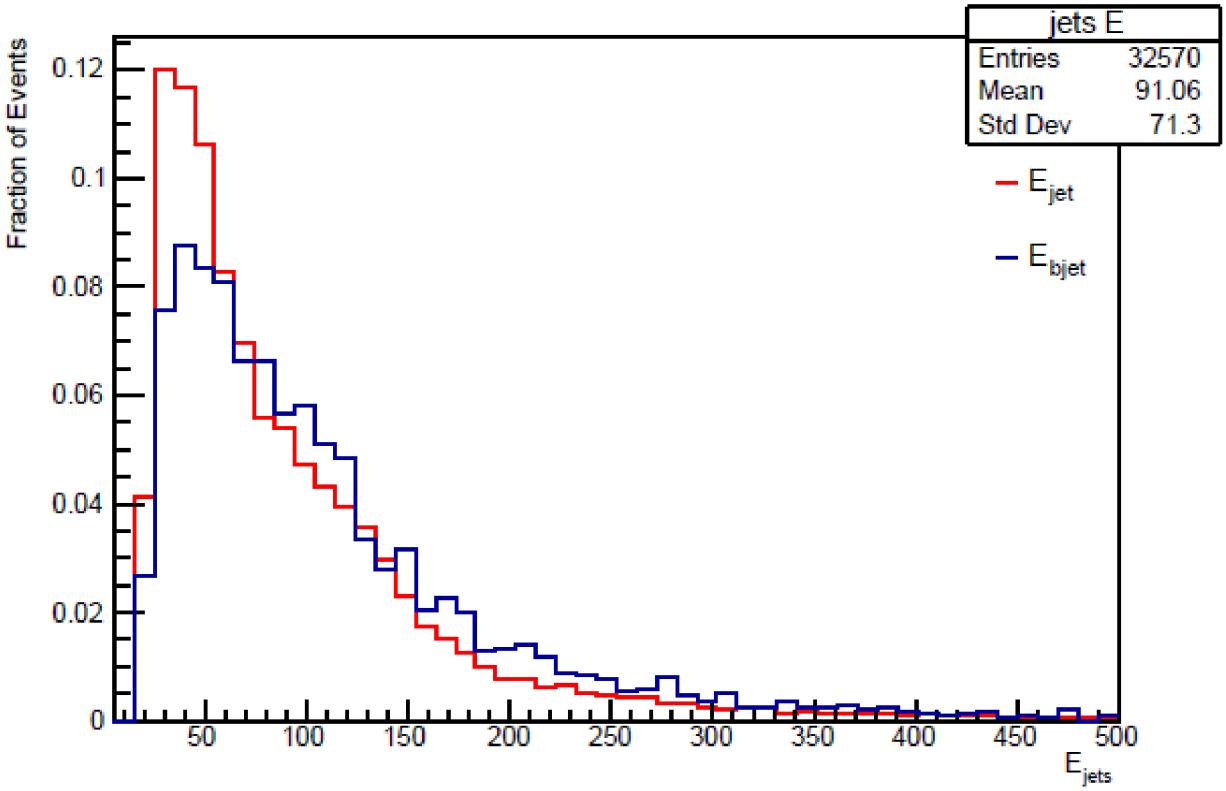

Figure 5.7: Normalized histogram of the E of light jets and b jets in the top-quark enriched sample from ATLAS p-Pb collisions.

As can be seen from Figures 5.3-5.7 there are some differences between the properties of light jets and b jets. The histograms show that b jets have a greater transverse momentum, energy and the pseudorapidity profile also differs between light jets and b jets. Histograms showing properties separately (including ϕ angle) are given in the Appendix (Figures 5-12). The histograms, like the previous ones, have reasonable ranges and show the counts we expect. We can see that there are almost 7 times as many light jets as b jets.

5.2.3 Invariant mass reconstruction

We proceed to reconstruct the invariant mass, we already know which particles contribute to the mass, and we know the corresponding decay mode. Unlike muons, jets of any kind cannot be considered massless, and so the pseudorapidity formula cannot be used. So, we get the invariant mass by constructing fourvectors and the TLorentz vector class. Again, we will use the definitions in both spherical and Cartesian coordinates, for which we must convert the momentum components appropriately using formulae 4.1, 4.2 and 4.3. It is also important to consider only events with at least 4 jets (of which 2 are b jets) when reconstructing the mass.

Starting with an invariant mass of the two light jets, we move on to adding the b jet invariant mass to the invariant mass of two light jets. From each relevant event, we loop through the required 2 light jets and 2 b jets (preferably with the largest possible p_T) and store their properties in a C++ structure we define. We construct TLorentz vectors for the light jets and use the appropriate method to obtain the invariant mass, with which we fill the first histogram Figure 5.8. Then we add a b jet which has a smaller distance to pair of light jets in the η-φ plane. This property is called ΔR and quantifies the angular separation between two particles or objects. It can be calculated as follows:

$$\Delta R = \sqrt{(\Delta\eta^2 + \Delta\phi^2}. \tag{5.1}$$

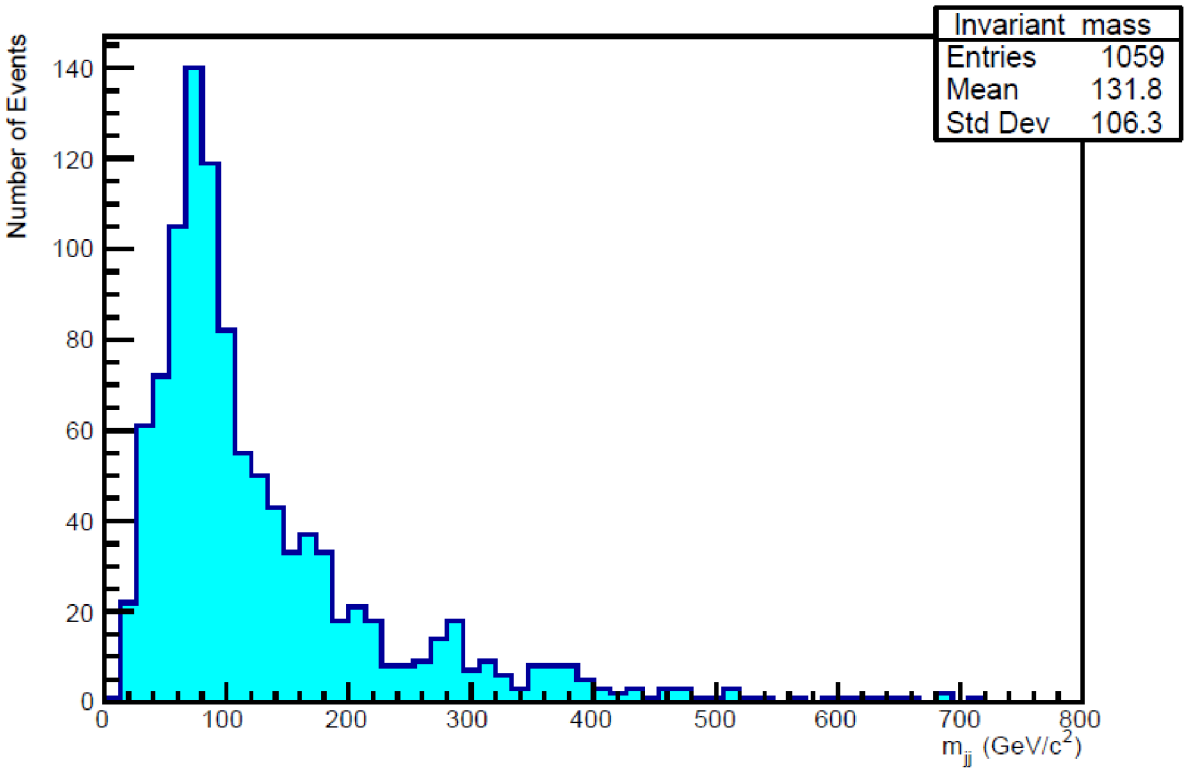

Figure 5.8: Histogram of the invariant mass of 2 light jets in the top-quark enriched sample from ATLAS p-Pb collisions.

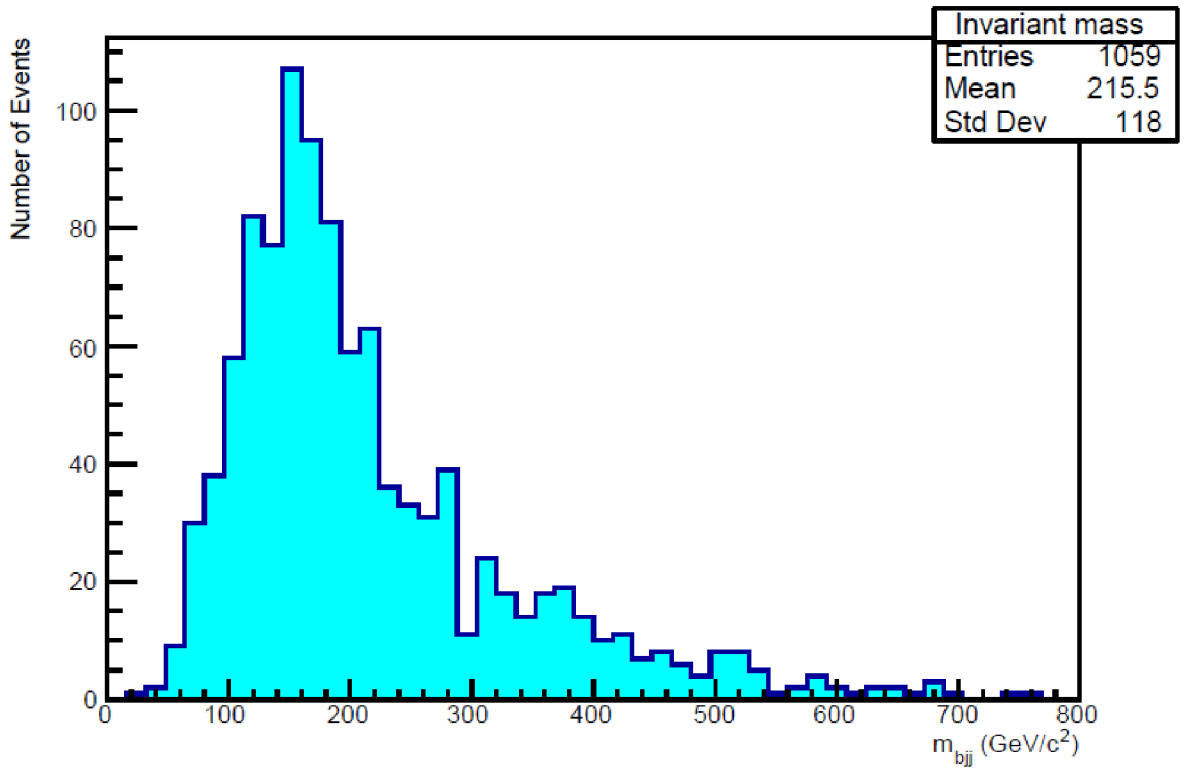

Figure 5.9: Histogram of the invariant mass of 2 light jets and b jet in the top-quark enriched sample from ATLAS p-Pb collisions.

Figures 5.8 and 5.9 show histograms of the invariant masses of the light jet pair alone and of the light jet pair with the addition of the b jet. The use of both TLorentzvector definitions leads to the same results, which we have checked as in Chapter 4.

5.3 Fitting of resonance peaks

When the reconstruction of the invariant masses of both cases is complete, we can extract the resonances and fit them with a Gaussian function, this time with an exponential function added to help describe the background. The value of mean parameter of the Gaussian function again gives us the value of the invariant mass and its uncertainty.

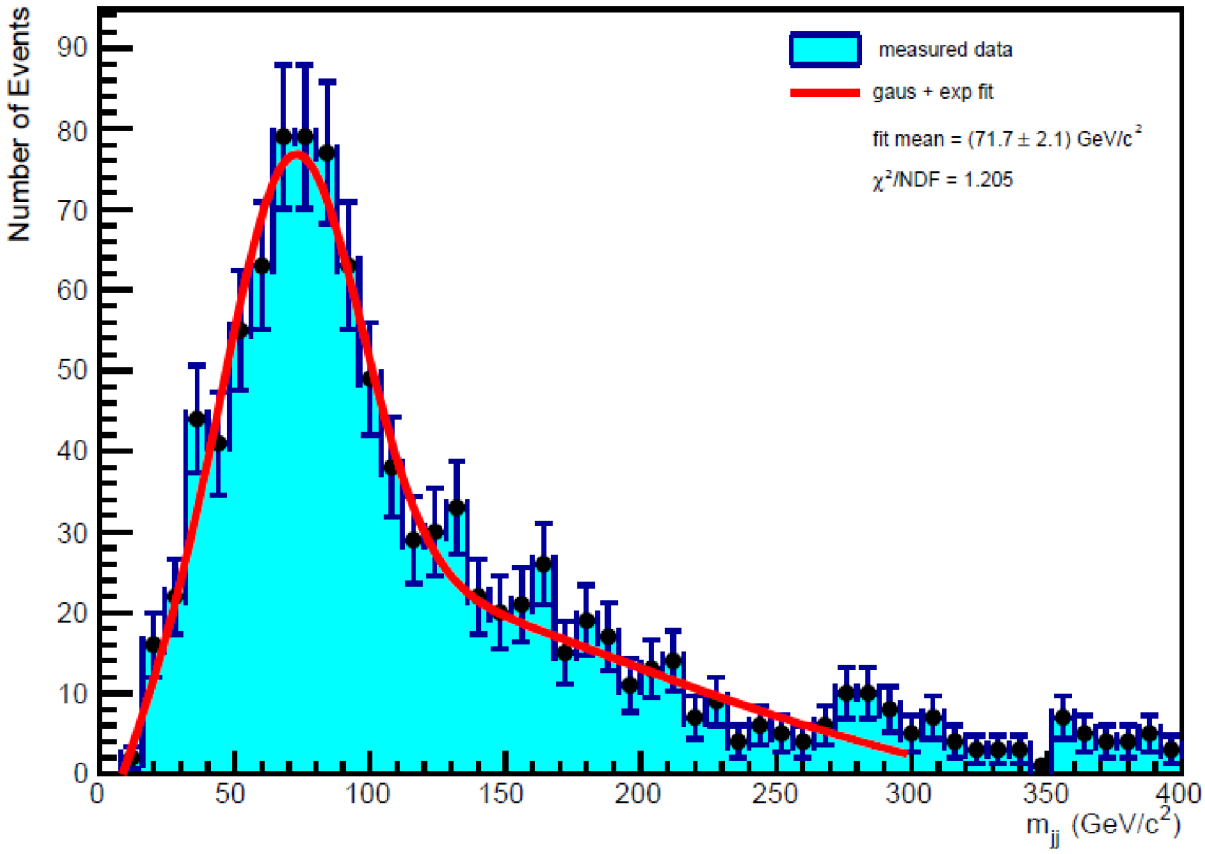

Figure 5.10: Histogram of the invariant mass of 2 light jets in the top-quark enriched sample from ATLAS p-Pb collisions, focusing on W boson mass peak localization and fitting. Also indicated is the fit quality in terms of the χ^2/NDF.

Beginning with the case of the invariant mass of two light jets. The W boson is one of the carriers of the weak interactions, which according to measurements by [8] has invariant mass $M_{\mathrm{PDG}} = (80.377 \pm 0.012)\ \mathrm{GeV/c}^2$. Our value determined by fitting is $M_{\mathrm{W}} = (71{,}7 \pm 2.1)\ \mathrm{GeV/c}^2$, which gives us the relative deviation about 12% with reference to M_{PDG}. The quality of the fit is given by the $\chi^2/\mathrm{NDF} = 1.205$. The W boson decays into hadrons in (67.47 ± 0.27) % cases according to [8].

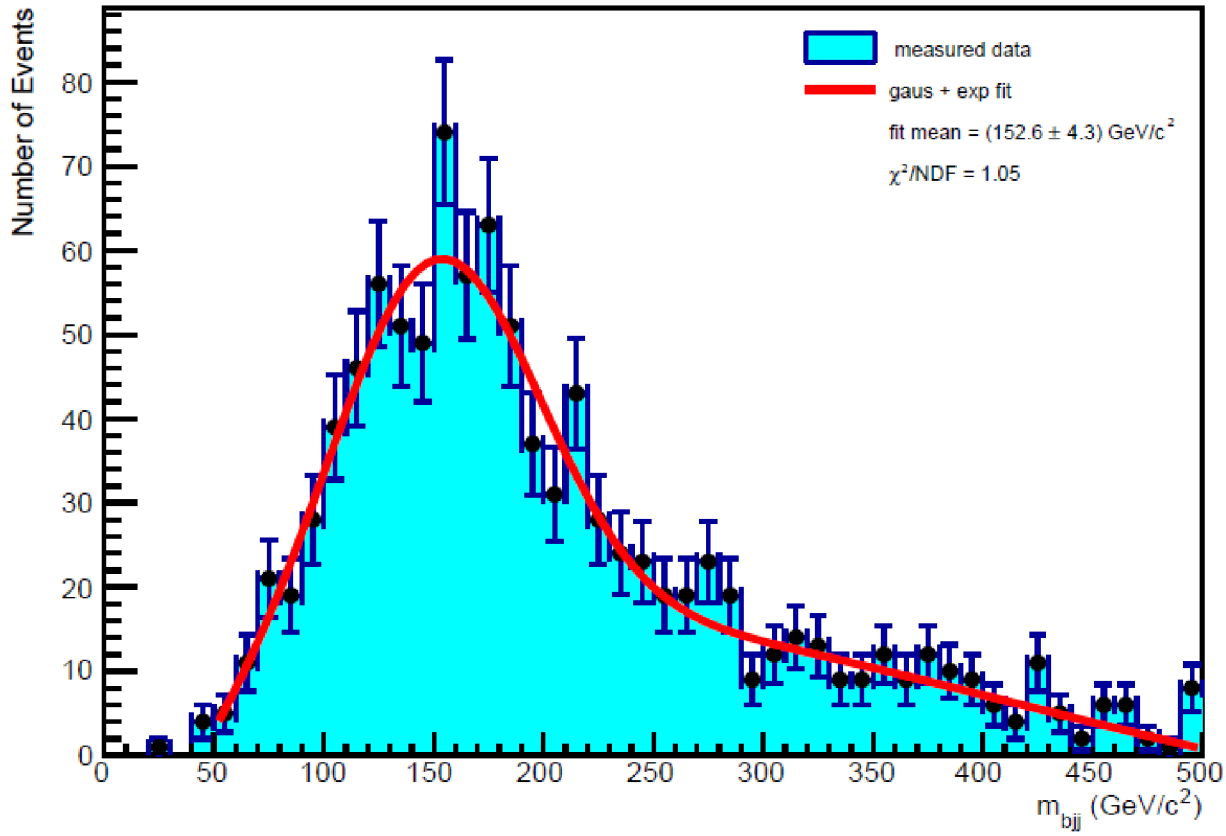

Figure 5.11: Histogram of the invariant mass of 2 light jets and the b jet in the top-quark enriched sample from ATLAS p-Pb collisions, focusing on top quark mass peak localization and fitting. Also indicated is the fit quality in terms of the χ^2/NDF.

The top quark, the heaviest of all quarks and the most studied particle today, has an invariant mass according to the measurement by [8] $M_{\mathrm{PDG}} = (172.69 \pm 0.030)\ \mathrm{GeV/c}^2$, our value determined by fitting is $M_{\mathrm{t}} = (152.6 \pm 4.3)\ \mathrm{GeV/c}^2$, which gives us the relative deviation about 13% with reference to M_{PDG}. The quality of fit is given by the $\chi^2/\mathrm{NDF} = 1.05$.

Conclusion

The aim of this bachelor thesis was to learn the techniques of invariant mass reconstruction and resonance peak identification by analyzing selected data from the ATLAS experiment at the LHC collider at CERN. The first chapter focuses on an introduction to elementary particles and their interactions. The second chapter briefly introduces the ATLAS experiment and its coordinate system. The third chapter is devoted to invariant mass and its calculation, and the fourth and fifth chapters are the actual analysis of the preselected data samples.

Data samples from proton and heavy ion collisions were studied using custom programs written in the C++ environment with the ROOT tool and libraries for thorough processing and analysis. By correctly applying the pseudorapidity formula and constructing fourvectors, analysis successfully calculated the invariant masses using multiple approaches. It also accurately located, fitted, and identified distinct resonance peaks in the di-μ data sample, extending its application to the more complex data sample of top quark pair decays.

Bibliography

1. Brun, R. and F. Rademakers. *ROOT - An Object-Oriented Data Analysis Framework.* 1997; Available from: https://root.cern/.

2. Braibant, S., G. Giacomelli, and M. Spurio, *Particles and Fundamental Interactions: An Introduction to Particle Physics*. 2011: Springer Netherlands. ISBN 9400724632.

3. Griffiths, D., *Introduction to Elementary Particles*. Second, Revised Edition ed. 2008, USA: WlLEY-VCH Verlag GmbH & Co. ISBN 978-3-527-40601-2.

4. Galbraith, D. and C. Burgard, *UX: Standard Model of the Standard Model*. 2012. Available from: https://davidgalbraith.org/portfolio/ux-standard-model-of-the-standard-model/.

5. Cottingham, W.N. and D.A. Greenwood, *AN INTRODUCTION TO THE STANDARD MODEL OF PARTICLE PHYSICS*. 2007, Cambridge University Press: United States of America. p. 295. ISBN 978-0-511-27377-3.

6. Woithe, J., G.J. Wiener, and F.F.V.d. Veken, *Let's have a coffee with the Standard Model of particle physics! et al* 2017 Phys. Educ. **52** 034 001.

7. Nave, C.R. *HyperPhysics*. 2017; Available from: http://hyperphysics.phy-astr.gsu.edu/hbase/index.html.

8. R.L. Workman *et al*. (Particle Data Group), Prog. Theor. Exp. Phys. **2022**, 083C01 (2022) and 2023 update.

9. *The ATLAS Experiment at the CERN Large Hadron Collider*. The ATLAS Collaboration *et al* 2008 JINST **3** S08003.

10. Grupen, Claus. *Particle Detectors*. Second edition. Cambridge University Press 2008. ISBN 9780511534966.

11. Schott, M. and M. Dunford, *Review of single vector boson production in pp collisions at s√=7 TeV. Eur. Phys. J. C* **74**, 2916 (2014). https://doi.org/10.1140/epjc/s10052-014-2916-1.

12. Neutelings, I., *Pseudorapidity*, in *TikZ.net*. 2021 Available from: https://tikz.net/axis2d_pseudorapidity/.

13. Thulasidharan and Lekshmi, *J/ψ,Y and Z studies with CERN Open Data.* 2018. DOI:10.13140/RG.2.2.20146.66245..

14. Sirunyan, A. *et al. Observation of the Z → ψ ℓ + ℓ − Decay in p p Collisions at s = 13 TeV.* Physical Review Letters, 2018. **121**. DOI:10.1103/PhysRevLett.121.141801

15. Department of Physics of the Faculty IV at the University of Siegen *Top-quark pair production*. 2020; Available from: https://www.hep.physik.uni-siegen.de.

16. Vermilion, Christopher. (2011). *Jet Substructure at the Large Hadron Collider*. [arXiv:1101.1335 [hep-ph]].

17. Paganini, Michela. (2017). *Machine Learning Algorithms for b-Jet Tagging at the ATLAS Experiment.* Journal of Physics: Conference Series. **1085**. DOI: 10.1088/1742-6596/1085/4/042031.

Appendix

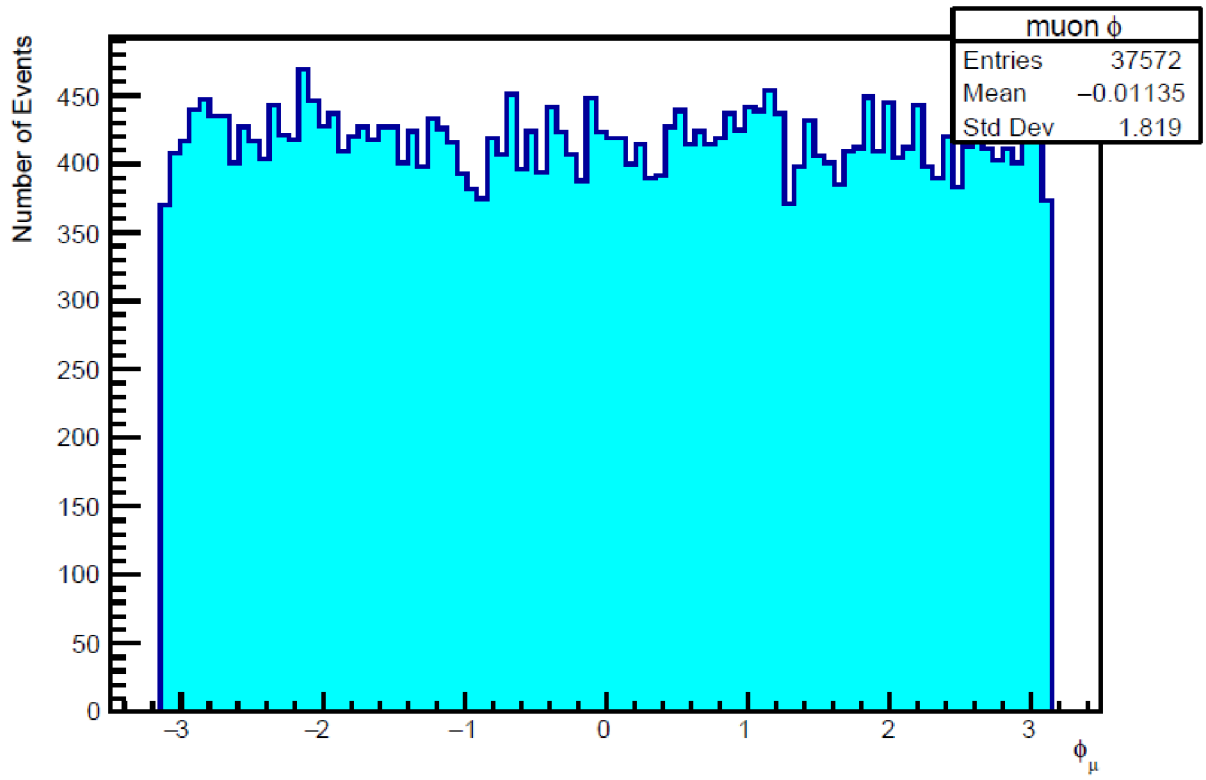

Figure 1: Histogram of the ϕ of muons in the di-μ sample from ATLAS p-Pb collisions.

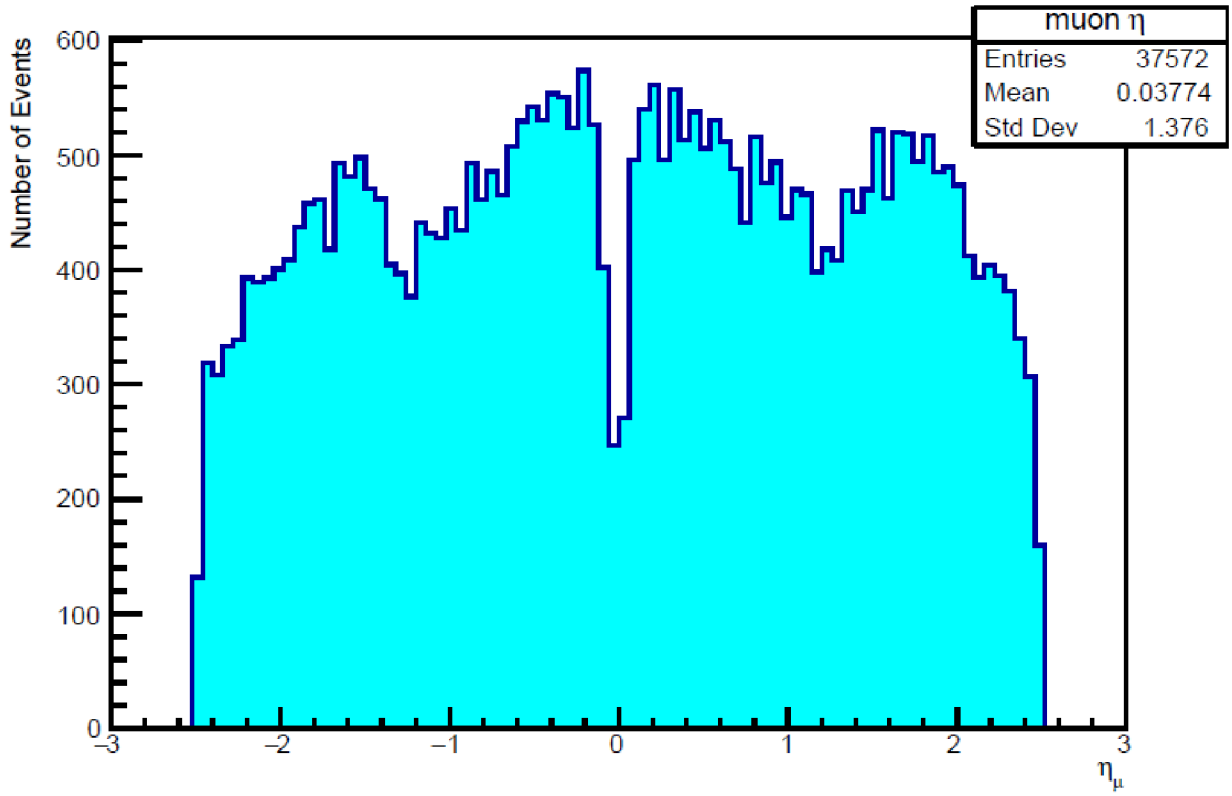

Figure 2: Histogram of the η of muons in the di-μ sample from ATLAS p-Pb collisions.

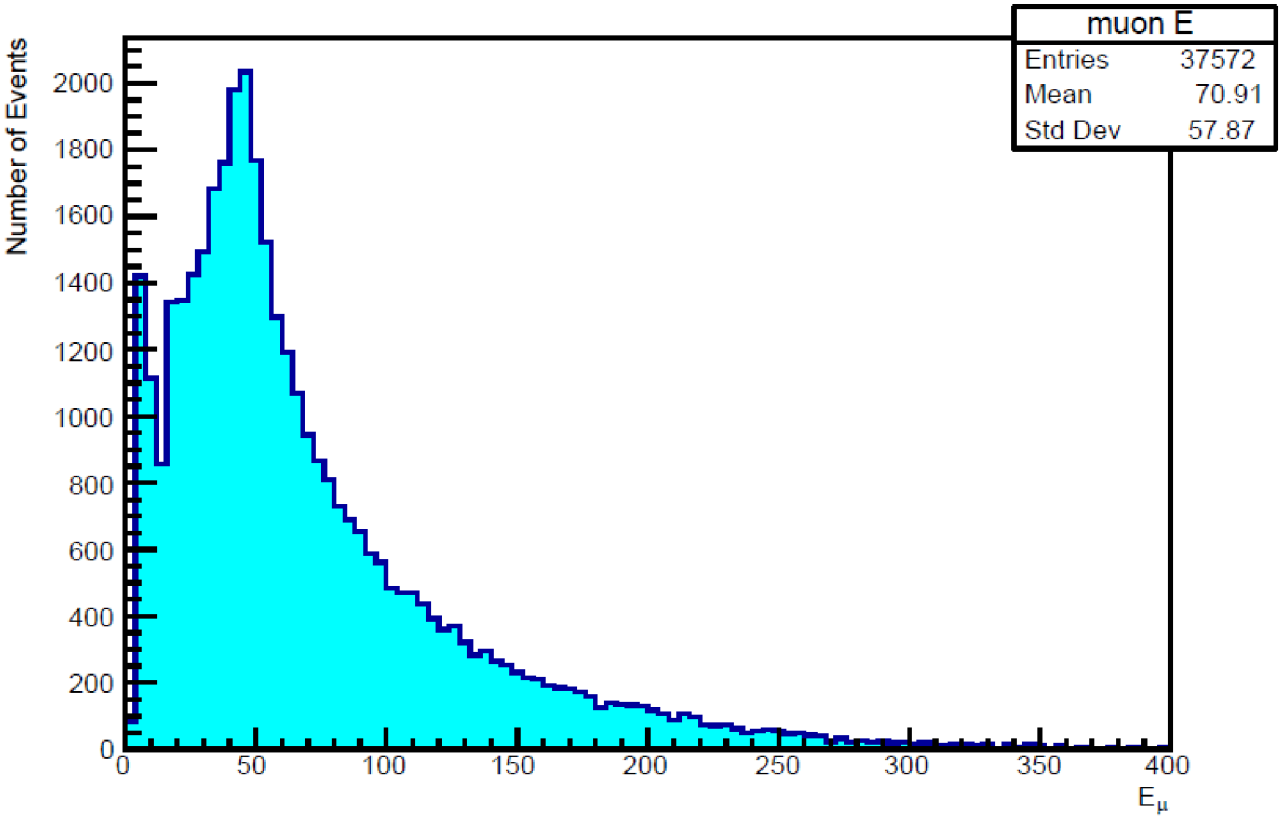

Figure 3: Histogram of the E of muons in the di-μ sample from ATLAS p-Pb collisions.

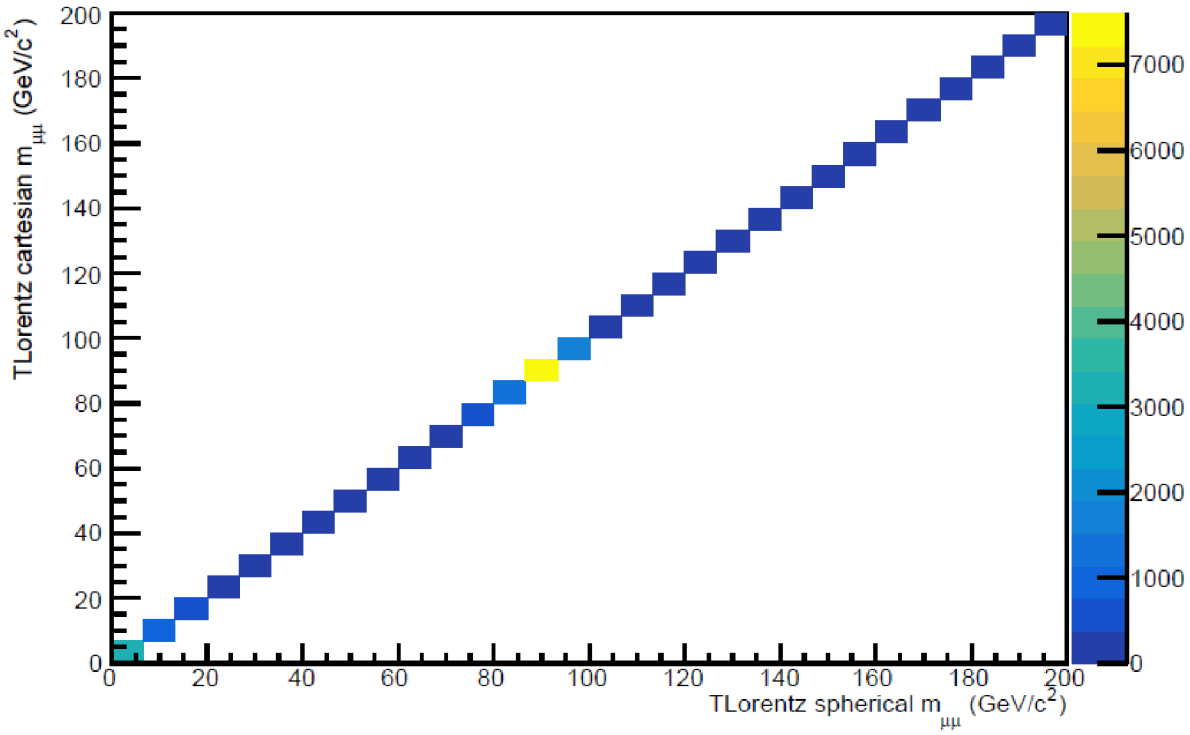

Figure 4: 2D histogram of the invariant masses of muon pairs using and TLorentzvetor (p_x, p_y, p_z, E). and TLorentzvetor (p_T, η, ϕ, E) in the di-μ sample from ATLAS p-Pb collisions.

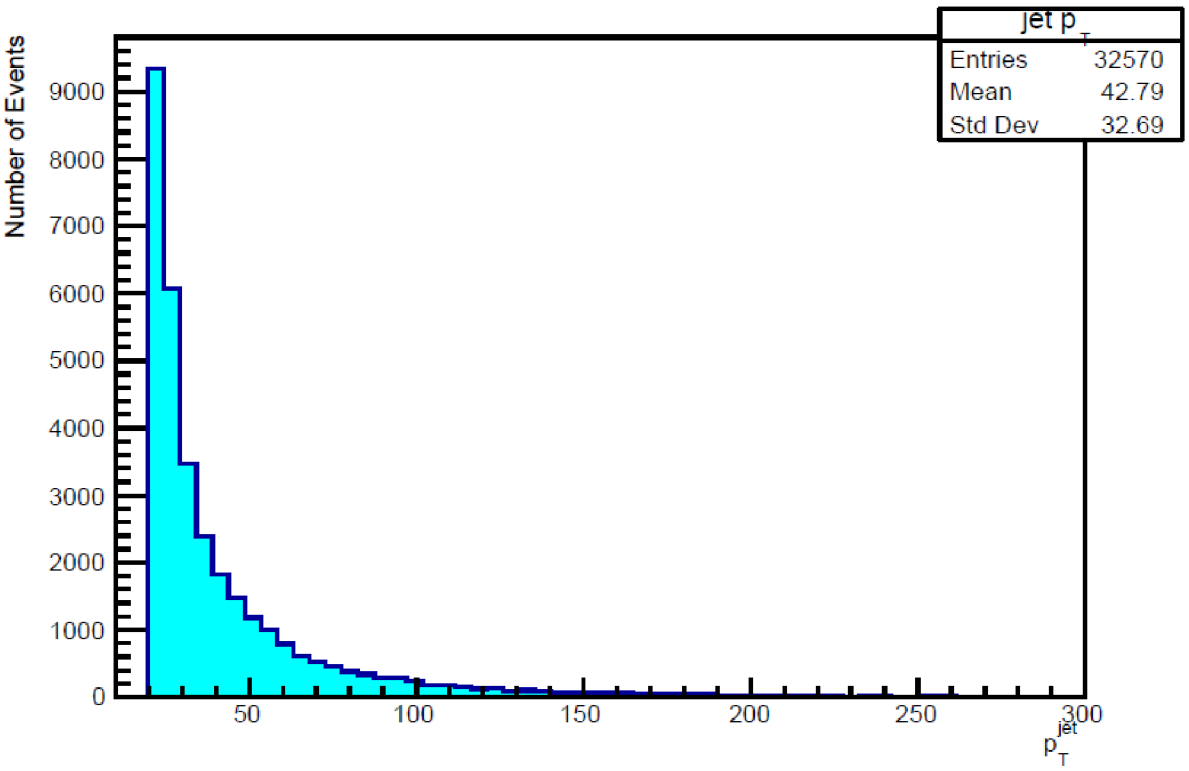

Figure 5: Histogram of the p_{T} of light jets in the top-quark enriched sample from ATLAS p-Pb collisions.

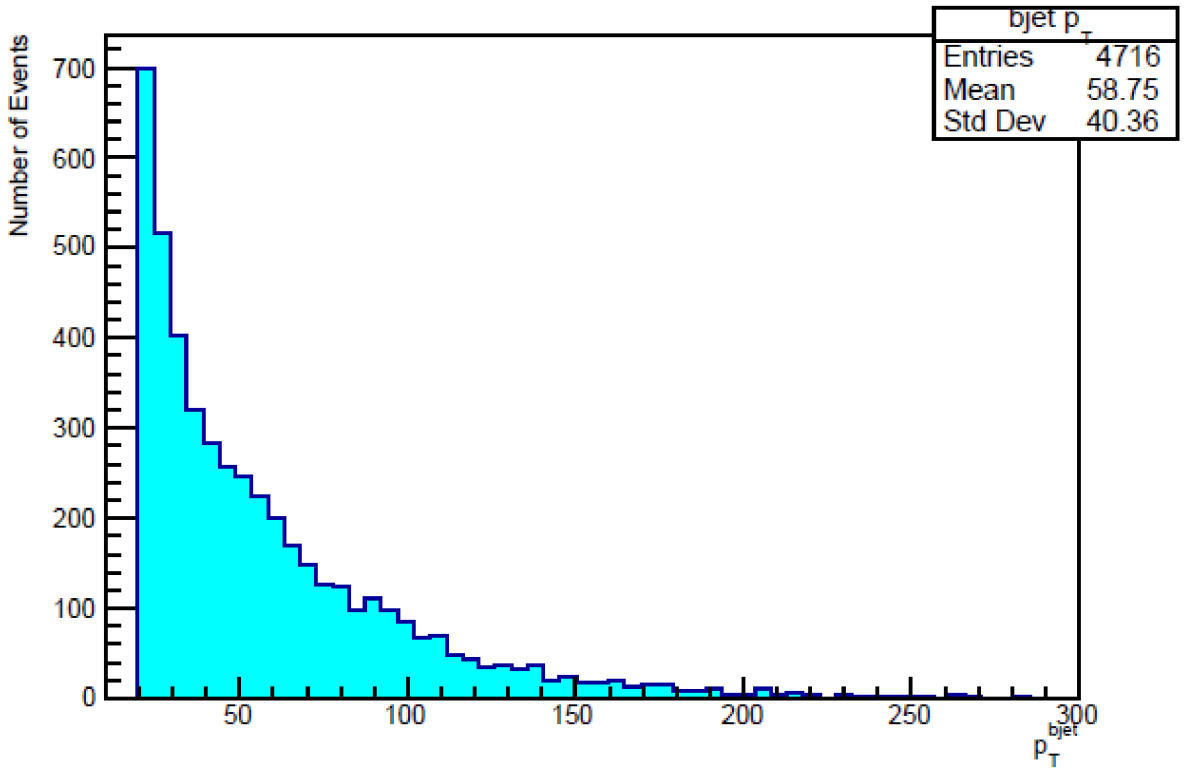

Figure 6: Histogram of the p_{T} of b jets in the top-quark enriched sample from ATLAS p-Pb collisions.

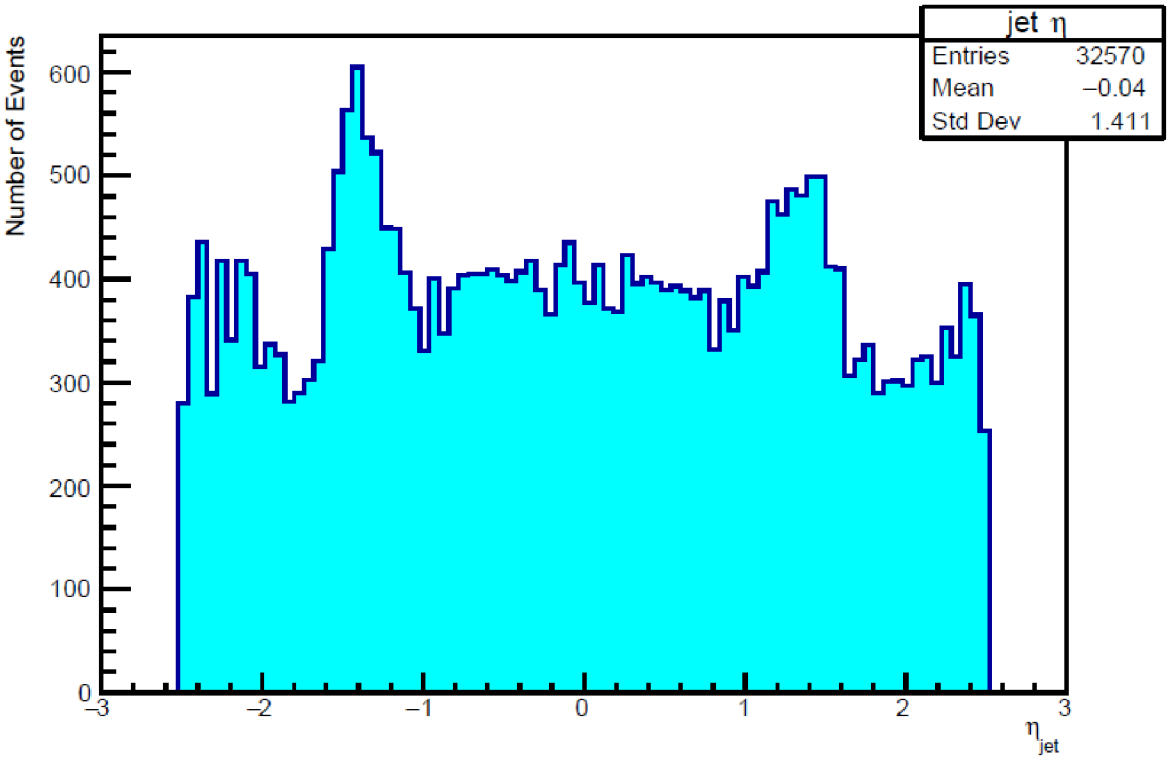

Figure 7: Histogram of the η of light jets in the top-quark enriched sample from ATLAS p-Pb collisions.

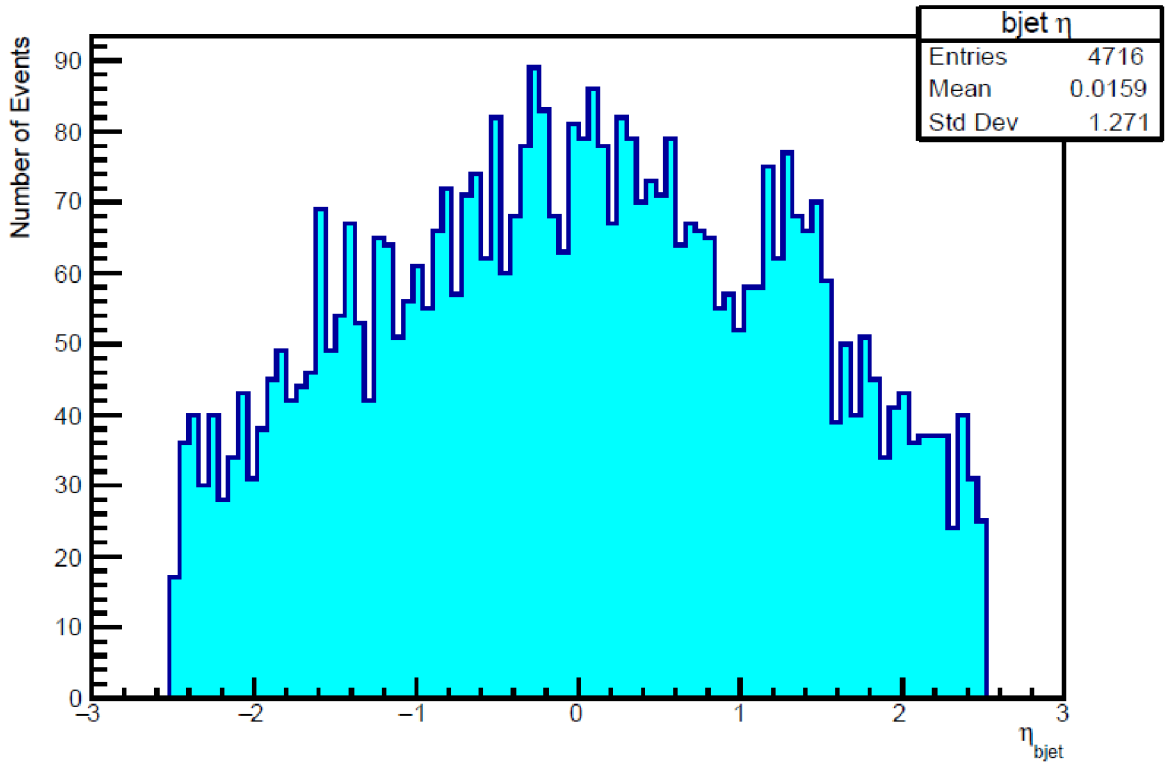

Figure 8: Histogram of the η of b jets in the top-quark enriched sample from ATLAS p-Pb collisions.

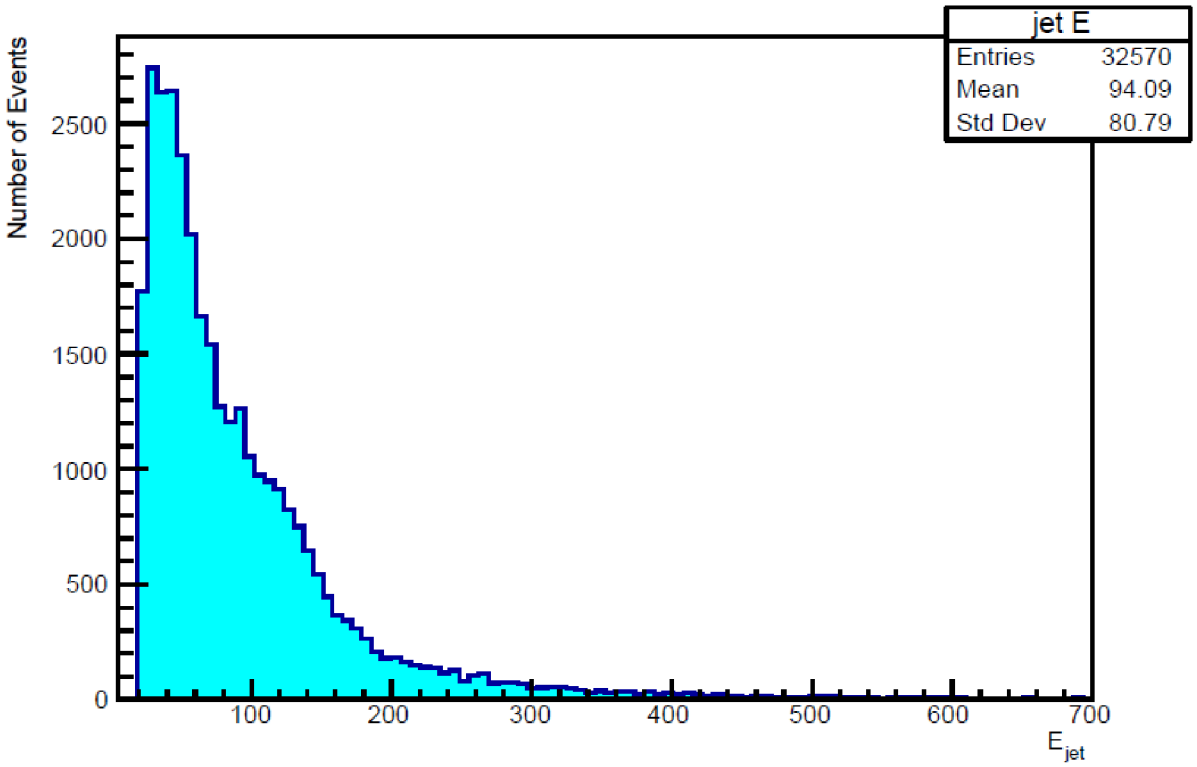

Figure 9: Histogram of the E of light jets in the top-quark enriched sample from ATLAS p-Pb collisions.

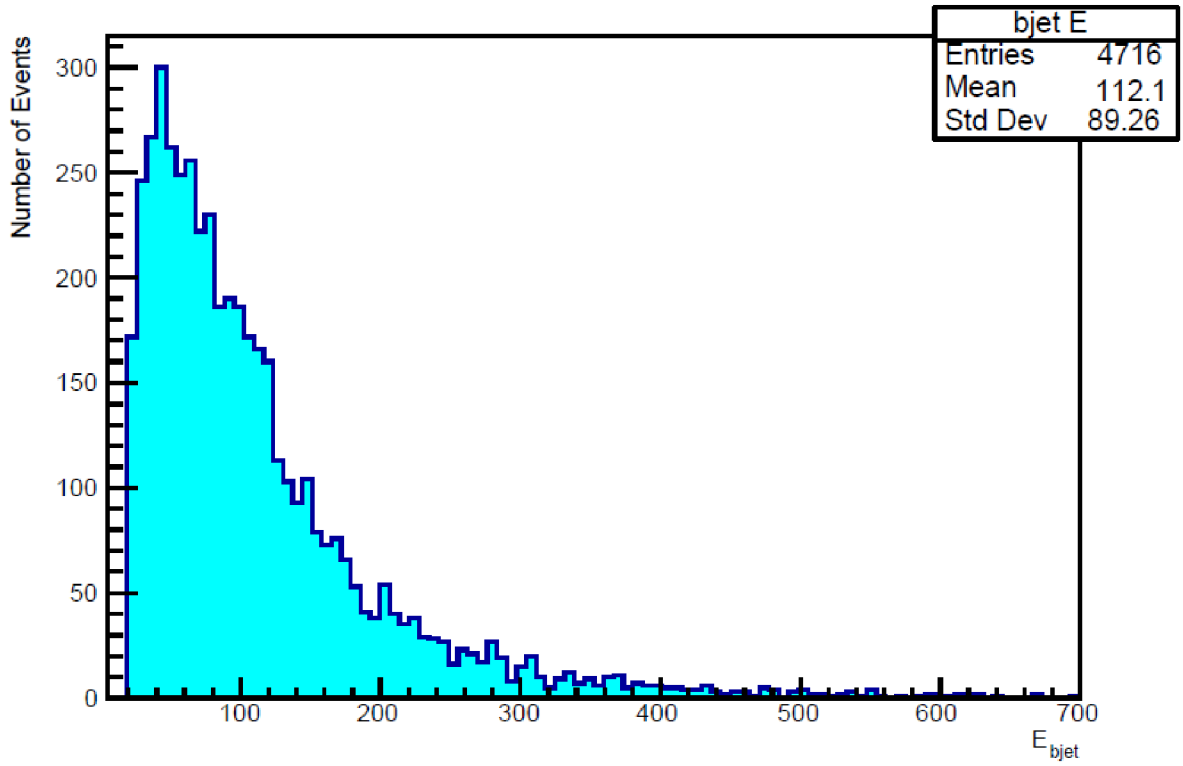

Figure 10: Histogram of the E of b jets in the top-quark enriched sample from ATLAS p-Pb collisions.

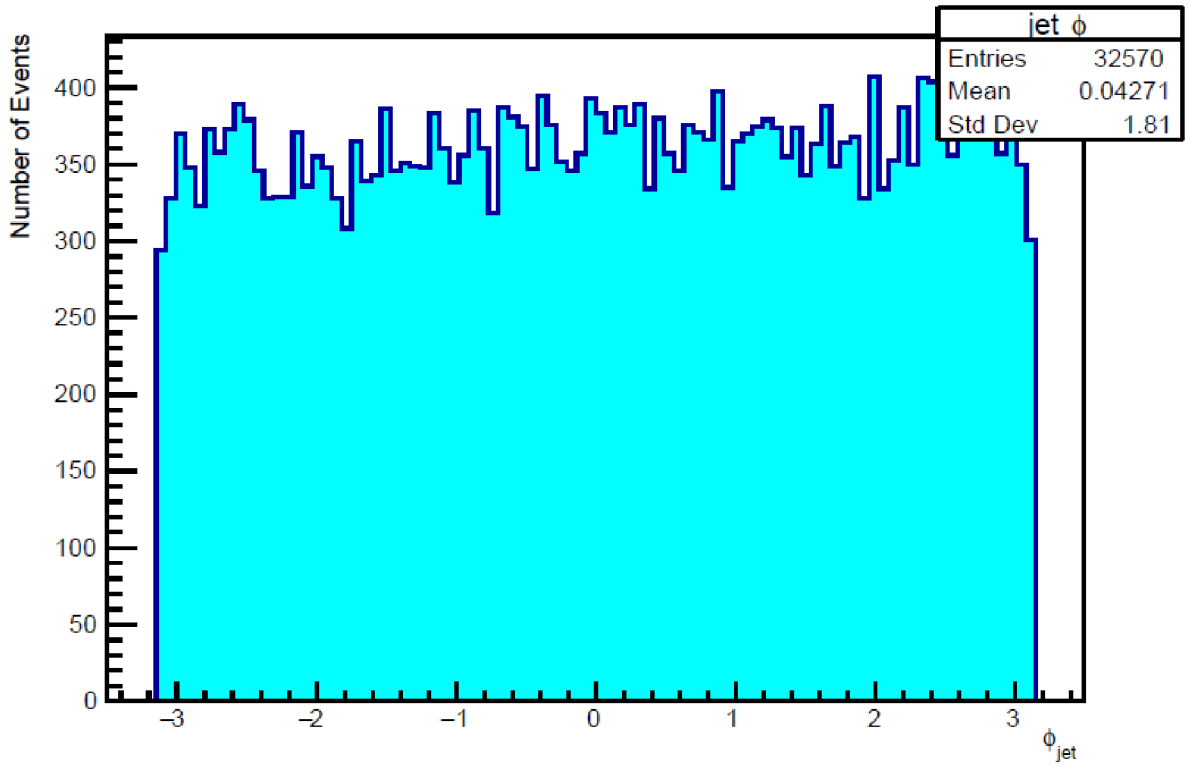

Figure 11: Histogram of the ϕ of light jets in the top-quark enriched sample from ATLAS p-Pb collisions.

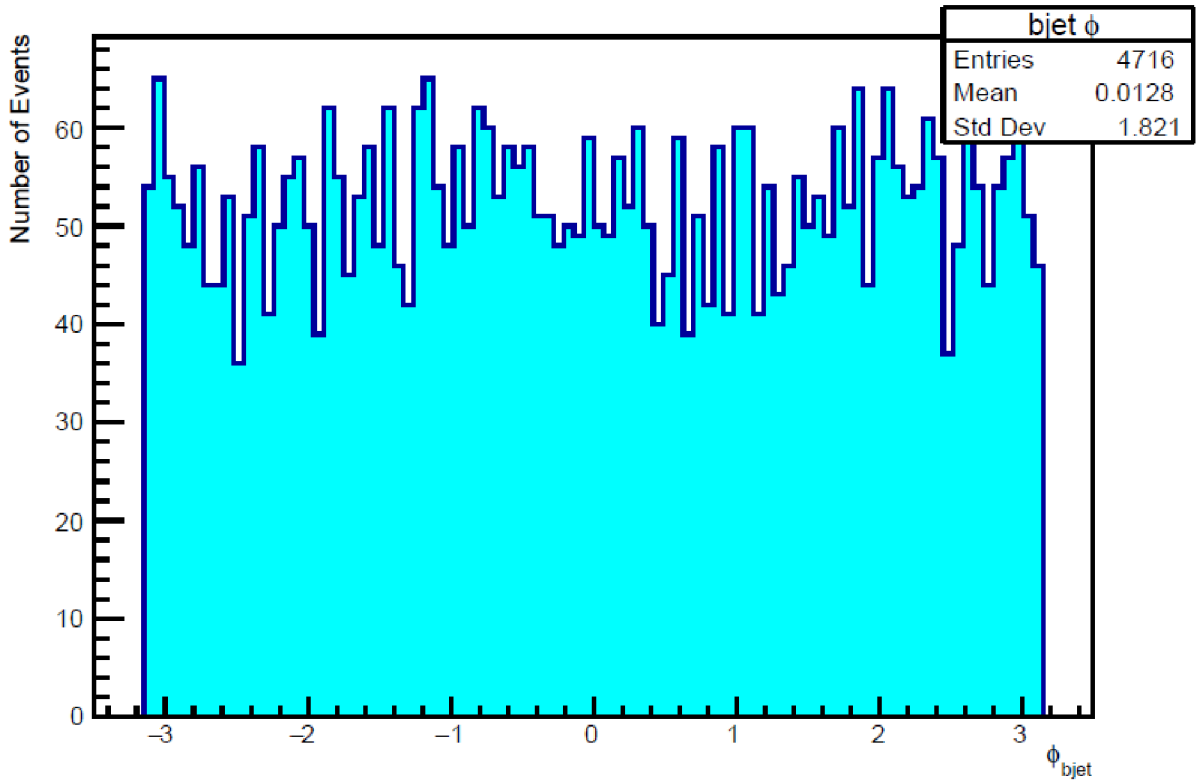

Figure 12: Histogram of the ϕ of b jets in the top-quark enriched sample from ATLAS p-Pb collisions.